Movement Disorders
Vol. 24, No. 9, 2009, pp. 1312–1318

Cerebellar Involvement in Progressive Supranuclear Palsy: A Clinicopathological Study

Masato Kanazawa, MD,[1] Takayoshi Shimohata, MD, PhD,[1]* Yasuko Toyoshima, MD, PhD,[2] Mari Tada, MD,[1,2] Akiyoshi Kakita, MD, PhD,[2,3] Takashi Morita, MD, PhD,[4] Tetsutaro Ozawa, MD, PhD,[1] Hitoshi Takahashi, MD, PhD,[2] and Masatoyo Nishizawa, MD, PhD[1]

[1]*Department of Neurology, Brain Research Institute, Niigata University, Niigata, Japan*
[2]*Department of Pathology, Brain Research Institute, Niigata University, Niigata, Japan*
[3]*Department of Pathological Neuroscience, Resource Branch for Brain Disease Research CBBR, Brain Research Institute, Niigata University, Niigata, Japan*
[4]*Department of Pathology, Shinrakuen Hospital, Niigata, Japan*

Abstract: The clinical heterogeneity of progressive supranuclear palsy (PSP), which is classified as classic Richardson's syndrome (RS) and PSP-Parkinsonism (PSP-P), has been previously discussed. We retrospectively analyzed 22 consecutive Japanese patients with pathologically proven PSP to investigate the clinicopathological heterogeneity. We investigated the clinical features both early in and at any time during the disease course. The pathological severities of neuronal loss with gliosis and tau pathology were also evaluated. On the basis of the clinical features, 10 patients were categorized as having RS, and 8 were categorized as having PSP-P. Four patients presenting with cerebellar ataxia or cerebral cortical signs were categorized as having unclassifiable PSP. Among them, 3 developed cerebellar ataxia as the initial and principal symptom. Notably, tau-positive inclusion bodies in Purkinje cells were significantly more frequently observed in the patients with cerebellar ataxia than in those without cerebellar ataxia. All the patients with cerebellar ataxia exhibited more neuronal loss with gliosis and higher densities of coiled bodies in the cerebellar dentate nucleus than those without cerebellar ataxia. This study confirms the wide spectrum of clinicopathological manifestations associated with PSP regardless of different ethnic origin, and demonstrates that PSP patients manifest cerebellar ataxia. © 2009 Movement Disorder Society

Key words: progressive supranuclear palsy; spinocerebellar ataxias; Parkinson's disease; parkinsonian disorders

Progressive supranuclear palsy (PSP) is a disorder, which is clinically characterized by supranuclear gaze palsy, pseudobulbar palsy, nuchal dystonia, and dementia.[1] PSP patients sometimes develop Parkinsonism early in the disease course, making it difficult to differentiate PSP from Parkinson's disease (PD).[2] A recent study revealed that one-third of Caucasian patients with pathologically proven PSP develop Parkinsonism, which is characterized by asymmetric onset, tremor, bradykinesia, and levodopa responsiveness.[3] On the basis of these observations, two distinct clinical phenotypes—classic Richardson's syndrome (RS) and PSP-Parkinsonism (PSP-P)—have been proposed. Recent studies also demonstrated that PSP patients develop pure akinesia with gait freezing,[4] cerebral cortical signs,[5] and predominant frontal presentations.[6] In addition, a very recent study reported that pathological features of PSP and pallido-nigro-luysial atrophy (PNLA) were overlapped.[7] However, little is known about the clinicopathological relationships in unclassifiable PSP, in which cerebellar ataxia or cerebral cortical signs develop.

Pathological examinations of RS patients have revealed that subcortical regions such as the globus pallidus, subthalamic nucleus, and substantia nigra are

*Correspondence to: Takayoshi Shimohata, MD, PhD, Department of Neurology, Brain Research Institute, Niigata University, 1-757 Asahimachi-dori, Chuoku, Niigata, Niigata 951-8585, Japan.
E-mail: t-shimo@bri.niigata-u.ac.jp

Potential conflict of interest: Nothing to report.

Received 24 September 2008; Revised 25 December 2008; Accepted 9 March 2009

Published online 1 May 2009 in Wiley InterScience (www.interscience.wiley.com). DOI: 10.1002/mds.22583

the most affected.[8] The involvement of the cerebellar dentate nucleus varies in each patient, although the cerebellar cortex is spared.[9] The differences in the tau pathology as well as in the severity of neuronal loss with gliosis among the clinical subtypes of PSP should be determined, because the changes in tau pathology involving neurofibrillary tangles (NFTs), tufted astrocytes (TAs), and coiled bodies (CBs) have been considered pathognomonic features of PSP.[10]

In this study, we demonstrated the wide spectrum of clinicopathological manifestations in Japanese PSP patients. In addition, we demonstrated that PSP patients manifest cerebellar ataxia.

PATIENTS AND METHODS

Subjects

We retrospectively reviewed the clinical records of consecutive Japanese patients with pathologically proven PSP, which were donated to and stored in our institute from 1981 and 2007. The pathological diagnoses were made in accordance with the National Institute for Neurological Disorders and Stroke-the Society for Progressive Supranuclear Palsy (NINDS-SPSP) criteria and the presence of TAs.[8] The pathological diagnoses required the exclusion of histopathological findings including large or numerous infarcts, oligodendroglial argyrophilic inclusions, Pick bodies, astrocytic plaques, and neuropathological changes consistent with Alzheimer's disease and postencephalitic Parkinsonism. We also excluded patients who were not followed continuously by trained neurologists certified by the Japanese Society of Neurology.

Clinical Data Collection

We reviewed the clinical records to determine the age at onset, age at death, disease duration, gender, and clinical features, within 2 years of disease onset and at any time during the disease course. The patients were examined for the presence of supranuclear vertical gaze palsy, gait disturbance, falls, postural instability, cognitive decline, asymmetry of symptoms, L-dopa responsiveness, and tremor of any type. The clinical symptoms and signs were defined as previously described.[3] Tremor was defined as the recording of resting, postural, or intentional tremor. Regarding response to L-dopa, the patient and clinician's interpretation of subjective improvement was assessed from the case notes. We examined for the presence of cerebellar ataxia, which is defined as the presence of gait ataxia plus at least either of ataxic dysarthria, limb ataxia, or sustained gaze-evoked nystagmus, as is the case with the definition of cerebellar symptom in the consensus statement on the diagnosis of multiple system atrophy.[11] We also examined for the presence of cerebral cortical signs, which are defined as the presence of alien hand phenomenon, cortical sensory loss, ideomotor apraxia, constructional apraxia, dressing apraxia, apraxia of speech, aphasia, visual or sensory hemineglect, and focal or asymmetric myoclonus.

Clinical Subtypes of PSP Patients

We classified the PSP patients into three clinical subtypes on the basis of the definitions provided in previous reports.[3,12] RS is defined as the subtype characterized by supranuclear vertical gaze palsy, falls, postural instability, and cognitive decline predominantly within 2 years of disease onset; PSP-P is defined as the subtype without those features and with features including asymmetric onset, L-dopa responsiveness, and tremor; unclassifiable PSP is defined as the subtype in which the patients develop cerebellar ataxia or cerebral cortical signs, which are diagnostic exclusion criteria for PSP.[13]

Pathological Examination

In this study, formalin-fixed and paraffin-embedded tissue blocks of various brain regions of all the patients were used. Histological examination was performed on 4-μm-thick sections using several stains: hematoxylin–eosin, Gallyas–Braak, and immunostained by a mouse monoclonal antibody against phosphorylation-dependent tau (AT8; Innogenetics, Ghent, Belgium; 1:200).[14]

Evaluation of neuronal loss with gliosis and morphometric analysis of the densities of NFTs, TAs, and CBs in the substantia nigra, globus pallidus, subthalamic nucleus, superior colliculus, periaqueductal gray matter, cerebellar dentate nucleus, cerebellar cortex, and precentral gyrus were performed semiquantitatively using a four-point scale (0, absent; 1+, mild; 2+, moderate; 3+, severe pathology) as described.[10,15] When we recognized the different degrees of changes in an anatomical region (e.g., external segment of globus pallidus 1+ versus internal segment of globus pallidus 3+), we used severe (e.g., 3+) as the grading.[16] Finally, we compared the pathological severities of the analyzed sections among all the PSP subtypes. These analyses were carried out by one author (M.K.), who was blind to the clinical features of the patients.

Statistical Analyses

Results were expressed as mean ± standard deviation. Parametric data were analyzed using Student's *t*-test and one-way analysis of variance with a post hoc Bonferroni test. Comparisons of the differences in gender and pathological findings were performed using Fisher's test. Statistical analyses were performed using SPSS (*ver.* 12.0). A P value <0.05 was considered statistically significant.

RESULTS

Clinical Features

We investigated the clinical features of 22 patients with definite PSP (15 men, 68.2%, and 7 women). The age at disease onset was 67.3 ± 8.0 years, age at death was 74.5 ± 8.0 years, and disease duration was 7.2 ± 3.6 years. All the patients developed supranuclear vertical gaze palsy in the advanced stage (Table 1). Early in the disease course, asymmetric onset and tremor was observed in 9 and 5 of the 22 patients, respectively. L-dopa responsiveness was observed in 5 of 11 patients. Three patients developed cerebellar ataxia, both truncal and limb ataxia, and 2 developed cerebral cortical signs such as apraxia of speech and alien hand phenomenon.

On the basis of these clinical features, 10 patients (45.4%) were categorized as having RS and 8 patients (36.4%) as having PSP-P. The remaining 4 patients (18.2%) were categorized as having unclassifiable PSP. The early-stage clinical features of the patients in each category are summarized in Table 2. Eight of the 10 RS patients and 4 of the 8 PSP-P patients were male (P = 0.18). The duration of PSP-P was significantly longer than that of RS and unclassifiable PSP (P = 0.001 and 0.001, respectively).

TABLE 1. *Clinical features of 22 patients with definite PSP*

Clinical feature	First 2 yr	Entire disease course
Progressive course	22/22 (100%)	22/22 (100%)
Onset over 40 yr of age	22/22 (100%)	22/22 (100%)
Supranuclear vertical gaze palsy	9/20 (45.0%)	22/22 (100%)
Gait disturbance	19/21 (90.5%)	21/22 (95.5%)
Falls	15/21 (71.4%)	21/22 (95.5%)
Postural instability	9/19 (47.4%)	21/22 (95.5%)
Cognitive decline	7/21 (33.3%)	16/22 (76.2%)
Asymmetric onset	9/22 (40.9%)	(−)
L-dopa responsiveness	5/11 (45.5%)	5/15 (33.3%)
Tremor	5/22 (22.7%)	8/22 (36.4%)
Resting	4/22 (18.2%)	5/22 (22.7%)
Intentional	0/22 (0%)	0/22 (0%)
Postural	1/22 (4.5%)	3/22 (13.6%)
Cerebellar ataxia	3/20 (15.0%)	3/21 (14.3%)
Truncal	3/20 (15.0%)	3/21 (14.3%)
Limb	3/20 (15.0%)	3/21 (14.3%)
Cerebral cortical signs	2/22 (9.1%)	2/22 (9.1%)

The table shows the frequencies of each clinical feature within 2 yr of disease onset and for the entire disease course.

Clinical Features of Unclassifiable PSP Patients

Three (Patients 1–3) developed cerebellar ataxia as gait ataxia and limb ataxia (Table 3). One (Patient 1) developed cerebellar ataxia as the initial symptom before supranuclear vertical gaze palsy and cognitive decline. Two (Patients 2 and 3) developed both cerebellar ataxia and cardinal features of PSP simultaneously. The antemortem diagnosis of Patient 1 and 2 was spinocerebellar degeneration. One (Patient 3) also showed alien hand phenomenon and asymmetric onset of rigidity. None of these patients were diagnosed as having PSP before their death because cerebellar ataxia was one of the exclusion criteria of NINDS-SPSP.[13] One (Patient 4) developed only apraxia of speech and dressing apraxia early in the disease course, but developed supranuclear vertical gaze palsy and became prone to falls in the advanced stage. All the unclassifiable PSP patients developed cardinal features of PSP during the disease course. No patients presenting with pure akinesia or frontal presentations were observed in our cohort.

Pathological Features of RS and PSP-P

We compared the severities of neuronal loss with gliosis between PSP-P and RS patients. We found that 7 of the 8 PSP-P patients as well as 5 of the 10 RS patients showed severe neuronal loss with gliosis in the substantia nigra (P = 0.09). Additionally, we found that 5 of the 6 PSP-P patients, in contrast to only one of the 8 RS patients, showed severe neuronal loss with gliosis in the subthalamic nucleus (P = 0.006). Although there were no apparent differences in pathological severity in the other examined regions, we did not detect Lewy bodies in the substantia nigra and dorsal vagal nucleus, which are the most affected regions in PD. We also did not detect axonal spheroids that were consistent with PNLA.

We also compared the severity of tau pathology between PSP-P and RS patients. The NFT and CB comparison revealed that the PSP-P patients tended to have less severe tau pathology in the substantia nigra, subthalamic nucleus, and periaqueductal gray matter than the RS patients, although the TA comparison did not reveal apparent differences (data not shown).

Pathological Features of Unclassifiable PSP Patients

We next investigated the pathological features of unclassifiable PSP patients. We compared the

TABLE 2. *Clinical features of PSP patients within 2 yr of disease onset*

Clinical feature	RS	PSP-P	Unclassifiable PSP
Number	10	8	4
Male(%)	80.0	50.0	75.0
Age at onset (yr)	69.3 ± 8.0	64.0 ± 9.4	69.0 ± 4.2
Age at death (yr)	74.4 ± 8.4	74.9 ± 9.9	73.8 ± 3.6
Disease duration (yr)	5.2 ± 2.3[a]	10.8 ± 2.6	4.8 ± 1.0[a]
Supranuclear vertical gaze palsy	6/10 (60.0%)	1/6 (25.0%)	2/4 (50.0%)
Gait disturbance	9/10 (90.0%)	7/7 (100%)	3/4 (75.0%)
Falls	10/10 (100%)	2/7 (28.6%)	3/4 (75.0%)
Postural instability	6/9 (66.7%)	1/6 (16.7%)	2/4 (50.0%)
Cognitive decline	5/9 (55.6%)	1/8 (12.5%)	1/4 (25.0%)
Asymmetric onset	1/10 (10.0%)	6/8 (75.0%)	2/4 (50.0%)
L-dopa responsiveness	0/5 (0%)	5/6 (83.3%)	NA
Tremor	0/10 (0%)	5/8 (62.5%)	0/4 (0%)
Cerebellar ataxia	0/10 (0%)	0/6 (0%)	3/4 (75.0%)
Cerebral cortical signs	0/10 (0%)	0/8 (0%)	2/4 (50.0%)

[a]$P < 0.01$ vs. patients with PSP-P. RS, Richardson's syndrome; PSP-P, progressive supranuclear palsy-parkinsonism; NA, not administered.

pathological severities of the cerebellar dentate nucleus and cerebellar cortex between 3 patients with cerebellar ataxia (Patients 1–3) and the remaining patients without cerebellar ataxia. The disease durations for the patients with and without cerebellar ataxia were 4.3 ± 0.6 years and 7.6 ± 3.7 years, respectively (P = 0.14). All 3 patients with cerebellar ataxia revealed more severe neuronal loss with gliosis (Fig. 1A, Table 4) and higher densities of CBs (Fig. 1B, Table 4) in the cerebellar dentate nucleus compared with RS and PSP-P patients. Two of the 3 patients with cerebellar ataxia showed a small number of TAs, while 3 of the 19 patients without cerebellar ataxia showed mild pathology of TAs in the cerebellar dentate nucleus (P = 0.12). In the cerebellar sections of patients with cerebellar ataxia, we found granular immuno-reactivity for AT8 antibody in the cytoplasm of a small proportion of the Purkinje cells (Fig. 1C,D). By Gallyas–Braak silver staining, we confirmed argyrophilic profiles (Fig. 1E), with variable intensity, of the tau-labeled granular

TABLE 3. *Clinical features of patients with unclassifiable PSP within 2 yr of disease onset and at any time during the disease course*

	Patient			
	1	2	3	4
First 2 yr				
Sex	F	M	M	M
Age at onset (yr)	64	72	73	67
Supranuclear vertical gaze palsy	–	+	+	–
Gait disturbance	+	+	+	–
Falls	+	+	+	–
Postural instability	+	+	–	–
Cognitive decline	–	–	+	–
Asymmetric onset	+	–	+	–
L-dopa responsiveness	NA	NA	NA	NA
Tremor	–	–	–	–
Cerebellar ataxia	T > L	T < L	T > L	–
Cerebral cortical signs	–	–	+	+
Entire disease course				
Disease duration (yr)	5	4	4	6
Supranuclear vertical gaze palsy	+	+	+	+
Gait disturbance	+	+	+	–
Falls	+	+	+	+
Postural instability	+	+	+	–
Cognitive decline	+	–	+	–
L-dopa responsiveness	NA	NA	NA	NA
Tremor	–	–	–	–
Cerebellar ataxia	T = L	T < L	T > L	–
Cerebral cortical signs	–	–	+	+

NA, not administrated; M, male; and F, female; T, truncal ataxia; L, limb ataxia.

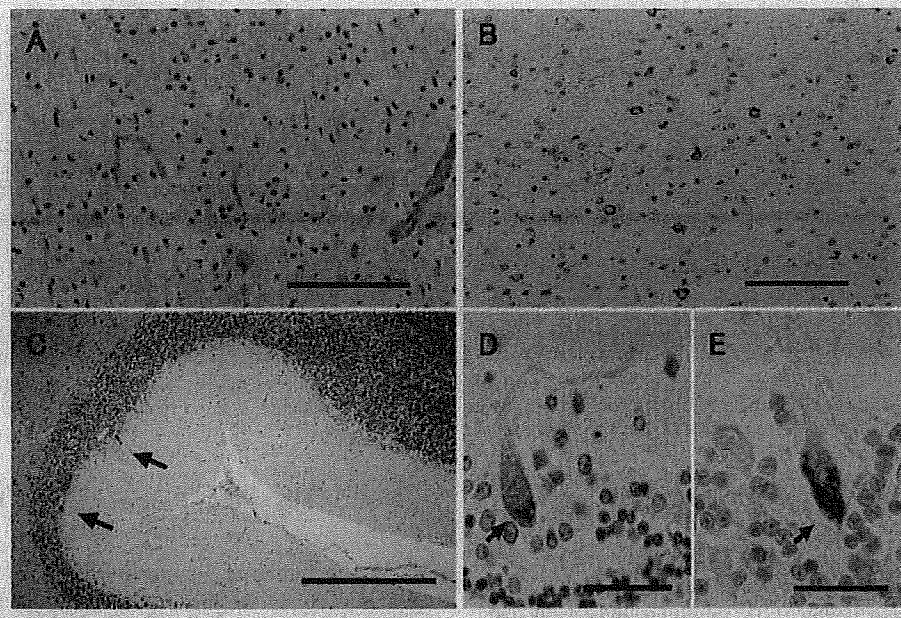

FIG. 1. Histopathological features of the cerebellar dentate nucleus (**A**, **B**) and cortex (**C**–**E**) of PSP patients with cerebellar ataxia. Neuronal loss and gliosis (A), and scattered coiled bodies (B) are seen. Low-power image of a tau-immunostained section showing two labeled Purkinje cells (C: arrows). High-power magnifications of Purkinje cells (arrows) demonstrating granular, tau-positive (**D**), and argyrophilic (**E**) profiles in the cytoplasm. A: hematoxylin–eosin stain; B–D: AT8 immunostain; E: Gallyas–Braak silver stain. Bars = 100 μm in A and B, 500 μm in C, and 25 μm in D and E. [Color figure can be viewed in the online issue, which is available at www.interscience.wiley.com.]

inclusions. The Purkinje cells with the inclusions were shrunk. Interestingly, we saw such inclusions in all 3 patients with cerebellar ataxia, whereas we encountered only 5 out of the 19 patients without cerebellar ataxia ($P = 0.036$).

We finally compared the pathological severities of the precentral gyrus between the 2 patients with cerebral cortical signs and 19 patients without them. The disease duration for the patients with cerebral cortical signs was 5.0 ± 1.4 years, vs. 7.4 ± 3.7 years for the patients without cerebral cortical signs ($P = 0.38$). Both patients with cerebral cortical signs revealed superficial spongiosis and moderate neuronal loss with gliosis ($P = 0.071$), and higher densities of CBs ($P = 0.071$) in the precentral gyrus, whereas only 4 of 19 patients without cerebral cortical signs revealed such severe pathology (Fig. 2A,B). We also evaluated the density of TAs in the precentral gyrus and found that both patients with cerebral cortical signs had very high TA density, whereas 7 of the 19 patients without cerebral cortical signs had very high TA density ($P = 0.17$).

DISCUSSION

Clinicopathological Features of PSP-P

Our study demonstrates that approximately one–third of the PSP patients in our Japanese cohort were categorized as having PSP-P. These patients showed no gender differences and a long disease duration compared with the RS patients, which is consistent with the findings reported in a previous study.[3] It was difficult to differentiate these patients from the patients with PD early in the disease course, although we could eventually differentiate them because the PSP-P patients also developed supranuclear vertical gaze palsy several years after the disease onset, which is consistent with previous descriptions.[5] Supranuclear

TABLE 4. *Cerebellar dentate nucleus in RS, PSP-P, and PSP patients with cerebellar ataxia*

		Severe	Moderate	Mild	Absent
Neuronal loss with gliosis					
RS	(N = 10)	3	6	1	0
PSP-P	(N = 8)	4	2	2	0
PSP-Cbll	(N = 3)	3	0	0	0
Densities of coiled bodies					
RS	(N = 10)	0	1	4	5
PSP-P	(N = 8)	0	0	3	5
PSP-Cbll	(N = 3)	1	1	1	0

The differences in pathological severities of neuronal loss with gliosis and densities of coiled bodies evaluated using the semiquantitative four-point scale among RS, PSP-P, and PSP patients with cerebellar ataxia are shown.

PSP-Cbll, PSP patients with cerebellar ataxia.

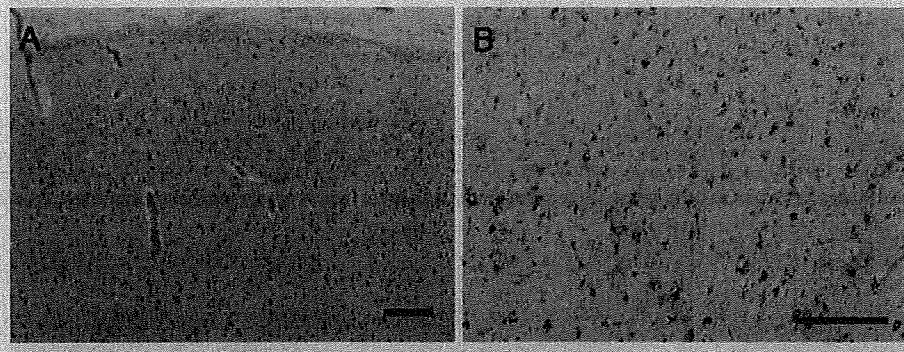

FIG. 2. Histopathological features of the precentral gyrus of PSP patients with cerebral cortical signs. Neuronal loss and superficial spongiosis (**A**) and scattered coiled bodies (**B**) are evident. A: hematoxylin–eosin stain. B: AT8 immunostain. Bar = 100 μm. [Color figure can be viewed in the online issue, which is available at www.interscience.wiley.com.]

vertical gaze palsy is considered an important symptom that differentiates PSP-P from PD.

Pathological examination revealed more severe neuronal loss with gliosis in the substantia nigra and subthalamic nucleus in the PSP-P patients than in the RS patients, which is consistent with the previous speculation that L-dopa responsiveness in PSP is prominent when the pathological process is primarily focused in the substantia nigra.[17] Although we speculated that the PSP-P patients would exhibit Lewy bodies because Lewy bodies were found coincidentally in ~10% of PSP patients,[18] we did not detect Lewy bodies during the pathological examinations. We consider that the PSP-P phenotype might not occur in association with the neurodegeneration relevant to α-synuclein.

Clinical Features of Unclassifiable PSP

We encountered patients presenting with cerebral cortical signs, who were clinically referred to as having corticobasal syndrome.[19] Previous studies have shown that patients with pathologically proven PSP develop cerebral cortical signs including ideomotor apraxia, alien hand phenomenon, and apraxia of speech.[5,20,21] Pathological investigation revealed that patients with cerebral cortical signs showed more severe neuronal loss with gliosis and higher densities of CBs in the precentral gyrus between the patients with and without cerebral cortical signs as described previously.[22] This finding might expand the phenotypic profile of PSP, to include PSP characterized by cerebral cortical signs as part of the clinical picture. However, we may not be able to evaluate these findings sufficiently, because frontal presentations and cognitive decline are not easily captured on standard tests of mental status unless specifically assessed.

Clinicopathological Features of PSP Patients With Cerebellar Ataxia

We encountered 3 patients presenting with cerebellar ataxia early in the disease course, who were diagnosed as having spinocerebellar degeneration, although cerebellar ataxia is one of diagnostic exclusion criteria for PSP.[13] However, the original report on PSP described 4 of 9 PSP patients who developed truncal and limb ataxia and one patient who developed truncal ataxia as an initial and principal symptom.[23] A PSP patient presenting with limb ataxia who exhibited neuronal loss of Purkinje cells have also been reported.[24] Cerebellar ataxia was demonstrated to be a rare symptom of PSP in a large case series of pathologically proven PSP.[3] However, Collins et al.[5] and Birdi et al.[17] reported that 8.3 and 6.3% of pathologically proven PSP patients developed cerebellar ataxia, respectively, although their reports described a small case series. These findings suggest that "PSP with cerebellar ataxia" is a clinical subtype of PSP.

This study also revealed that patients with cerebellar ataxia tended to have a higher number of tau-positive inclusion bodies in Purkinje cells than those without cerebellar ataxia, regardless of the shorter disease duration. We previously reported the presence of tau-positive inclusion bodies in Purkinje cells of PSP patients,[14] although little is known about the relationship between this pathological finding and clinical presentations. Although we speculated that patients with tau-positive inclusion bodies in Purkinje cells and degenerated dentate nucleus more easily develop cerebellar ataxia than those without them, we also encountered patients without cerebellar ataxia despite the presence of tau-positive inclusion bodies in Purkinje cells and severe degeneration of the dentate nucleus. In addition, semi-quantitative analyses of NFT and CBs

demonstrated that PSP-P patients tended to have lesser severity in substantia nigra, which are the most affected region in this subtype. The factors that influence the severity of tau pathology in PSP are unknown. Analyses of genetic backgrounds such as H2 haplotype [3,25] may enable us to understand the clinicopathological difference between RS and PSP-P. We speculated that the difference of degree of severities between tau pathology and neuronal loss might be explained by that of disease duration or H2 haplotype between two subtypes, although H2 haplotype is found in Caucasians but not in other population.[26] Further study is required to determine the effect of tau accumulation on neuronal loss in each subtype.

We evaluated pathological alterations in a semi-quantitative manner. A semi-quantitative assessment of neuronal loss with gliosis and tau pathology was performed, using an approach similar to that described by Dickson et al.[10] and Wenning et al.[15] To confirm the intra-rater reliability or the repeatability of the methods, further studies are needed.

Acknowledgments: The authors thank Drs. Y. Horikawa, M. Wakabayashi, T. Noda, S. Tokiguchi, R. Koike, T. Fujita, A. Honma, K. Kikugawa, and K. Sanpei for their contributions to this study. They also thank N. Kaneko, T. Tanabe, C. Tanda, and J. Takasaki for their technical assistance. Furthermore, the authors thank the patients and their families who made this research possible.

Author Roles: Conception and design: MK, TS, AK, HT, MN. Data acquisition: MK, TS, YT, MT, AK, TM. Drafting of manuscript: MK, TS. Editing of manuscript: TS, YT, AK, TO, HT, MN.

REFERENCES

1. Richardson JC, Steele JC, Olszewski J. Supranuclear ophthalmoplegia, pseudobulbar palsy, nuchal dystonia and dementia. Trans Am Neurol Assoc 1963;88:25–29.
2. Hughes AJ, Daniel SE, Lees AJ. Improved accuracy of clinical diagnosis of Lewy body Parkinson's disease. Neurology 2001; 57:1497–1499.
3. Williams DR, de Silva R, Paviour DC, et al. Characteristics of two distinct clinical phenotypes in pathologically proven progressive supranuclear palsy: Richardson's syndrome and PSP-Parkinsonism. Brain 2005;128:1247–1258.
4. Williams DR, Holton JL, Strand K, et al. Pure akinesia with gait freezing: A third clinical phenotype of progressive supranuclear palsy. Mov Disord 2007;22:2235–2241.
5. Collins SJ, Ahlskog JE, Parisi JE, et al. Progressive supranuclear palsy: neuropathologically based diagnostic clinical criteria. J Neurol Neurosurg Psychiatry 1995;58:167–173.
6. Kaat LD, Boon AJ, Kamphorst W, et al. Frontal presentation in progressive supranuclear palsy. Neurology 2007;69:723–729.
7. Ahmed Z, Josephs KA, Gonzalez J, et al. Clinical and neuropathologic features of progressive supranuclear palsy with severe pallido-nigro-luysial degeneration and axonal dystrophy. Brain 2008;131:460–472.
8. Litvan I, Hauw JJ, Bartko JJ, et al. Validity and reliability of the preliminary NINDS neuropathologic criteria for progressive supranuclear palsy and related disorders. J Neuropathol Exp Neurol 1996;55:97–105.
9. Dickson DW. Neuropathologic differentiation of progressive supranuclear palsy and corticobasal degeneration. J Neurol 1999;246(Suppl. 2):II6–II15.
10. Dickson DW, Rademakers R, Hutton ML. Progressive supranuclear palsy: pathology and genetics. Brain Pathol 2007;17:74–82.
11. Gilman S, Wenning GK, Low PA, et al. Second consensus statement on the diagnosis of multiple system atrophy. Neurology 2008;71:670–676.
12. Williams DR, Watt HC, Lees AJ. Predictors of falls and fractures in bradykinetic rigid syndromes: a retrospective study. J Neurol Neurosurg Psychiatry 2006;77:468–473.
13. Litvan I, Agid Y, Calne D, et al. Clinical research criteria for the diagnosis of progressive supranuclear palsy (Steele-Richardson-Olszewski syndrome): report of the NINDS-SPSP international workshop. Neurology 1996;47:1–9.
14. Piao YS, Hayashi S, Wakabayashi K, et al. Cerebellar cortical tau pathology in progressive supranuclear palsy and corticobasal degeneration. Acta Neuropathol (Berl) 2002;103:469–474.
15. Wenning GK, Seppi K, Tison F, et al. A novel grading scale for striatonigral degeneration (multiple system atrophy). J Neural Transm 2002;109:307–320.
16. Ozawa T, Paviour D, Quinn NP, et al. The spectrum of pathological involvement of the striatonigral and olivopontocerebellar systems in multiple system atrophy: clinicopathological correlations. Brain 2004;127:2657–2671.
17. Birdi S, Rajput AH, Fenton M, et al. Progressive supranuclear palsy diagnosis and confounding features: report on 16 autopsied cases. Mov Disord 2002;17:1255–1264.
18. Uchikado H, DelleDonne A, Ahmed Z, et al. Lewy bodies in progressive supranuclear palsy represent an independent disease process. J Neuropathol Exp Neurol 2006;65:387–395.
19. Tsuboi Y, Josephs KA, Boeve BF, et al. Increased tau burden in the cortices of progressive supranuclear palsy presenting with corticobasal syndrome. Mov Disord 2005;20:982–988.
20. Soliveri P, Piacentini S, Girotti F. Limb apraxia in corticobasal degeneration and progressive supranuclear palsy. Neurology 2005;64:448–453.
21. Josephs KA, Duffy JR, Strand EA, et al. Clinicopathological and imaging correlates of progressive aphasia and apraxia of speech. Brain 2006;129:1385–1398.
22. Josephs KA, Katsuse O, Beccano-Kelly DA, et al. Atypical progressive supranuclear palsy with corticospinal tract degeneration. J Neuropathol Exp Neurol 2006;65:396–405.
23. Steele JC, Richardson JC, Olszewski J. Progressive supranuclear palsy—a heterogeneous degeneration involving the brain stem, basal ganglia and cerebellum, with vertical gaze and pseudobulbar palsy, nuchal dystonia and dementia. Arch Neurol 1964; 10: 333–359.
24. Utsumi H, Abe K, Yoshii O, et al. A 71-year-old woman with progressive gait disturbance and dementia. No To Shinkei 1995; 47:295–307.
25. Williams DR, Holton JL, Strand C, et al. Pathological tau burden and distribution distinguishes progressive supranuclear palsy-Parkinsonism from Richardson's syndrome. Brain 2007;130:1566–1576.
26. Hardy J, Pittman A, Myers A, et al. Evidence suggesting that *Homo neanderthalensis* contributed the H2 *MAPT* haplotype to *Homo sapiens*. Biochem Soc Trans 2005;33:582–585.

Tract-by-Tract Morphometric and Diffusivity Analyses In Vivo of Spinocerebellar Degeneration

Kenshi Terajima, MD, PhD, Hitoshi Matsuzawa, MD, PhD, Takayoshi Shimohata, MD, PhD, Kouhei Akazawa, PhD, Masatoyo Nishizawa, MD, PhD, Tsutomu Nakada, MD, PhD

From the Center for Integrated Human Brain Science, Brain Research Institute, University of Niigata, Niigata, Japan (KT, HM, TN); Department of Neurology, Brain Research Institute, University of Niigata, Niigata, Japan (KT, TS, MN); Department of Medical Informatics, University of Niigata Medical and Dental Hospital, University of Niigata, Niigata, Japan (KT, KA).

ABSTRACT

BACKGROUND AND PURPOSE

Three-dimensional anisotropy contrast (3DAC) based on a periodically rotated overlapping parallel lines with enhanced reconstruction (PROPELLER) sequence on a 3.0T system is a new magnetic resonance imaging technique capable of providing images with significantly high anatomical resolution. The purpose of this study was to confirm whether this technique can characterize the degenerative processes in the brainstem of patients with spinocerebellar degeneration (SCD).

METHODS

3DAC images of 13 patients with multiple system atrophy with predominant cerebellar symptoms (MSA-C) and seven International Cooperative Ataxia Rating Scale (ICARS) score-matched patients with Machado-Joseph disease (MJD) were created using a diffusion-weighted PROPELLER sequence on a 3.0T system. The section of the middle pons was chosen for morphometric and diffusivity analyses.

RESULTS

The above analyses showed that atrophy and increased diffusivity of the ventral portion of the pons indicated MSA-C, whereas atrophy and increased diffusivity of the pontine tegmentum indicated MJD. Furthermore, ICARS scores significantly correlated with both the severities of the pontine atrophy and the mean diffusivity values of the ventral pontocerebellar tracts.

CONCLUSIONS

This study demonstrated that 3DAC PROPELLER on a 3.0T system enables in vivo "tract by tract" quantitative analysis of pontine degeneration in SCD.

Keywords: 3DAC, PROPELLER, diffusion-weighted imaging, morphometry, spinocerebellar degeneration.

Acceptance: Received January 15, 2008, and in revised form March 12, 2008. Accepted for publication April 12, 2008.

Correspondence: Address correspondence to Kenshi Terajima, MD, PhD, Department of Medical Informatics, University of Niigata Medical and Dental Hospital, 1 Asahimachi, Niigata 951-8520, Japan. E-mail: terajima@bri.niigata-u.ac.jp.

J Neuroimaging 2009;19:220-226.
DOI: 10.1111/j.1552-6569.2008.00273.x

Introduction

Three-dimensional anisotropy contrast (3DAC) is a magnetic resonance (MR) imaging technique for creating vector contrast fiber orientation weighted images from information on anisotropic diffusion mechanics in the central nervous system.[1-3] Several successful clinical applications of 3DAC have been reported.[4-8] However, spinocerebellar degeneration (SCD) is a challenging target to which this technique has been hardly applied. In general, SCD is characterized by the degeneration of nuclei and fiber tracts in the brainstem or cerebellum, which differ in degree or distribution according to the subtypes of the disease. Detailed information on the degenerative changes in SCD has so far been obtained mostly by postmortem pathological examination, because the required anatomical resolution is higher than those of other previous imaging methods. Recently, 3DAC based on periodically rotated overlapping parallel lines with enhanced reconstruction (PROPELLER) sequence on a 3.0T system has been developed.[9] This new imaging technique, which provides higher anatomical resolution and higher image contrast than conventional MR imaging, enables more detailed analysis of disease characteristics in the brainstem.

In this study, we applied this new technique to patients with SCD to confirm whether this technique can characterize in vivo degenerative processes in pontine tracts in two representative subtypes of SCD showing contrasting pathologies, namely, multiple system atrophy with predominant cerebellar symptoms (MSA-C) and Machado-Joseph disease (MJD). We performed morphometric and diffusivity analyses of pontine tract degeneration in such patients and compared the results with those of previous pathological and imaging studies. We also analyzed the relationship between the parameters obtained from these analyses and the cerebellar symptoms of the patients.

Methods

Patients and Normal Controls

Thirteen patients with probable MSA-C diagnosed using the consensus criteria of Gillman et al.,[10] 7 patients with genetically proven MJD, and 13 healthy volunteers as normal controls participated in this study. Written informed consent was obtained from all the participants in accordance with the human research guidelines of the Internal Review Board of the

Table 1. The Profile of Subjects Participated in This Study

	Normal	MSA-C	MJD
n (F/M)	13 (9/4)	13 (6/7)	7 (3/4)
Age	33.7 ± 18.5	61.6 ± 6.6	47.1 ± 17.1
Disease duration (y)		3.1 ± 1.9	9.3 ± 7.8
ICARS		37.6 ± 17.9	36.3 ± 18.3

Values are expressed as means ± standard deviations.
MSA-C = multiple system atrophy with predominant cerebellar symptoms; MJD = Machado-Joseph disease; ICARS = International Cooperative Ataxia Rating Scale.

University of Niigata. The severities of the cerebellar symptoms of the two patient groups were "clinically matched" using International Cooperative Ataxia Rating Scale (ICARS) scores.[11] The profiles of the subjects are summarized in Table 1.

Data Acquisition

A General Electric Signa 3.0T system (Waukesha, WI) with a quadrature head coil was used for all the imaging studies. Anisotropic diffusion-weighted axial images were obtained using a PROPELLER sequence[12,13] with the following parameter settings: field of view (FOV), 22 cm × 22 cm; matrix, 256 × 256; slice thickness, 5 mm with a 2.5 mm interslice gap; echo train length, 12; repetition time (TR), 4,000 msec; echo time (TE), 78.7 msec; and number of acquisitions (NEX), 3. The diffusion gradient (*b*-value, 1,100 sec/mm^2) was applied sequentially along the x-, y-, and z-axes, each of which corresponds to three orthogonal directions of the brain in the supine position (x: right to left, y: anterior to posterior, z: superior to inferior). The parameters for the motion probing gradient pulses were as follows: gradient strength, 3.6 g/cm; pulse duration, 19 msec; and time between the onsets of the first and second gradient pulses, 29 msec. Considering the specific absorption rate, the number of slices was limited to four. The total scanning time necessary to obtain four slice images was approximately 17 minutes.

Image Processing and Data Analysis

The 3DAC images were processed using a previously reported method.[5] Three primary colors–red, green, and blue–were assigned to the gray scale of the three anisotropic diffusion-weighted PROPELLER images on the x-, y-, and z-axes, respectively. These three color images were then combined pixel by pixel to form a single color image in a full color spectrum. The final images were displayed as negative images to obtain a one-to-one correlation between each of the three colors and their corresponding axes. This process effectively eliminates the isotropic components of the central nervous system, since the sum of the three primary colors of identical intensity results in a white out. In addition, the color frequency (hue) of each pixel reflects the direction of anisotropy, and the color intensity of each pixel provides the magnitude of the diffusivity. Furthermore, mean diffusivity (*MD*), that is, one-third of the trace of the apparent diffusion tensor, can be given by the average of the apparent diffusion coefficients measured on the three orthogonal x-, y-, and z-axes.[14]

Of the four slices of the acquired 3DAC images, we chose one slice of the pons containing bilateral intramedullary root entry zones of the fifth nerves and the fastigium of the fourth ventricle. On this slice, the following procedures including tract identification and morphometric and diffusivity analyses were performed automatically using in-house routines written in MATLAB (MathWorks, Natick, MA). First, red, green, and blue pixels were extracted using the hue ranges of their pixels, namely, 315-45°, 75-165°, and 195-285°, respectively. Next, these extracted pixels were divided into the following tracts: ventral portion of the pontocerebellar tract (VPCT), caudal portion of the pontocerebellar tract (CPCT), corticospinal tracts (CSTs), pontine tegmentum (PTG), and middle cerebellar peduncles (MCPs). Subsequently, the area of each identified tract between the bilateral MCPs was measured for the morphometric analysis, as shown in Figure 1. Finally, histograms of the hue and color intensity of the pixels of each identified tract were created. The pixels showing outlier values in either of the two histograms were excluded from the following diffusivity analyses, because such pixels were considered to have the partial volume effect of the surrounding cerebrospinal fluid. In the diffusivity analysis, the averaged *MD* value of all the pixels of each tract was calculated.

Statistical analysis was performed using SPSS for Windows version 14.0 (SPSS, Chicago, IL). The differences in the area measurements and *MD* values among the groups were compared using analysis of variance (ANOVA). Multiple pairwise comparisons were performed using Fisher's protected least significant difference method, with the overall alpha level set at .05. In all the patients with both MSA-C and MJD, the correlations of the area measurements or *MD* values of each tract with the ICARS scores of the patients were evaluated by Pearson's correlation test, where $P < .05$ was considered statistically significant.

Results

Figure 2 shows a representative 3DAC PROPELLER image on a 3.0T system of a normal brain. The 3DAC image of the pons has higher anatomical resolution and higher image contrast than a conventional fast spin-echo image, as shown in the comparison between Figures 2B and 2C. Furthermore, the 3DAC image of the pons can provide tract-specific information at least macroscopically similar to that obtained by conventional pathological examination, as shown in the comparison between Figures 2B and 2D.

Representative 3DAC images of a normal subject and the patients with MSA-C and MJD are shown in Figure 3. Marked atrophy of the pontine base, particularly VPCT, and severe atrophy of MCPs were observed in the MSA-C patients. On the other hand, the pontine base was relatively preserved and PTG showed atrophy in the MJD patients. These visual observations were confirmed by morphometric analysis, as shown in Table 2 and Figure 4A. Marked atrophy of all the pons and pontine tracts were observed in both the MSA-C and MJD patients compared with the normal controls. Furthermore, in the comparison between the two clinically matched patient groups, the atrophic changes in VPCT and CPCT were more pronounced

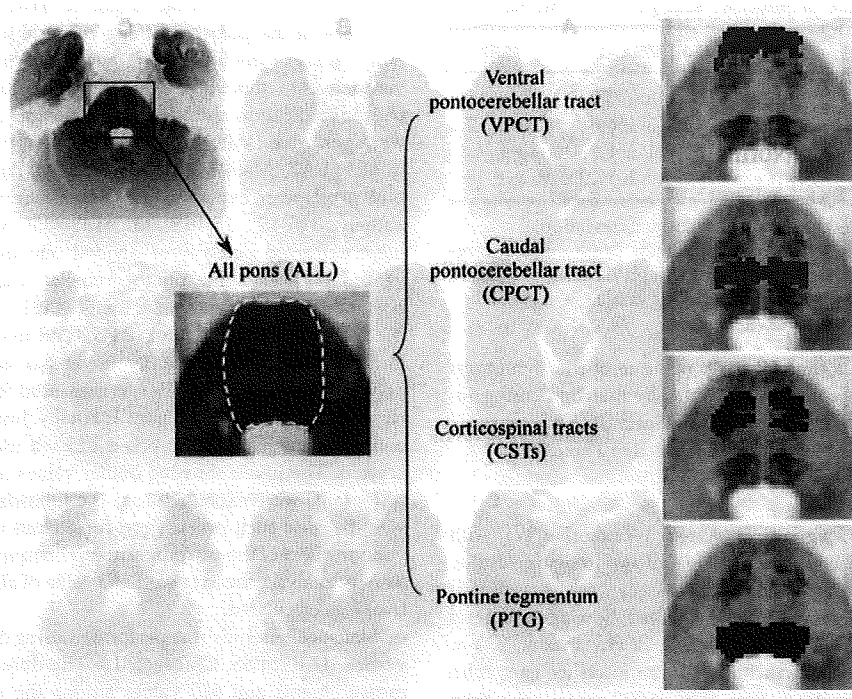

Fig 1. Identification of pontine tracts for morphometric and diffusivity analyses. In a 3DAC image of the middle pons, the following pontine tracts can be clearly recognized: ventral portion of the pontocerebellar tract (VPCT), caudal portion of the pontocerebellar tract (CPCT), corticospinal tracts (CSTs), and pontine tegmentum (PTG). The area and mean diffusivity of the identified tracts between the bilateral middle cerebellar peduncles were measured using in-house routines.

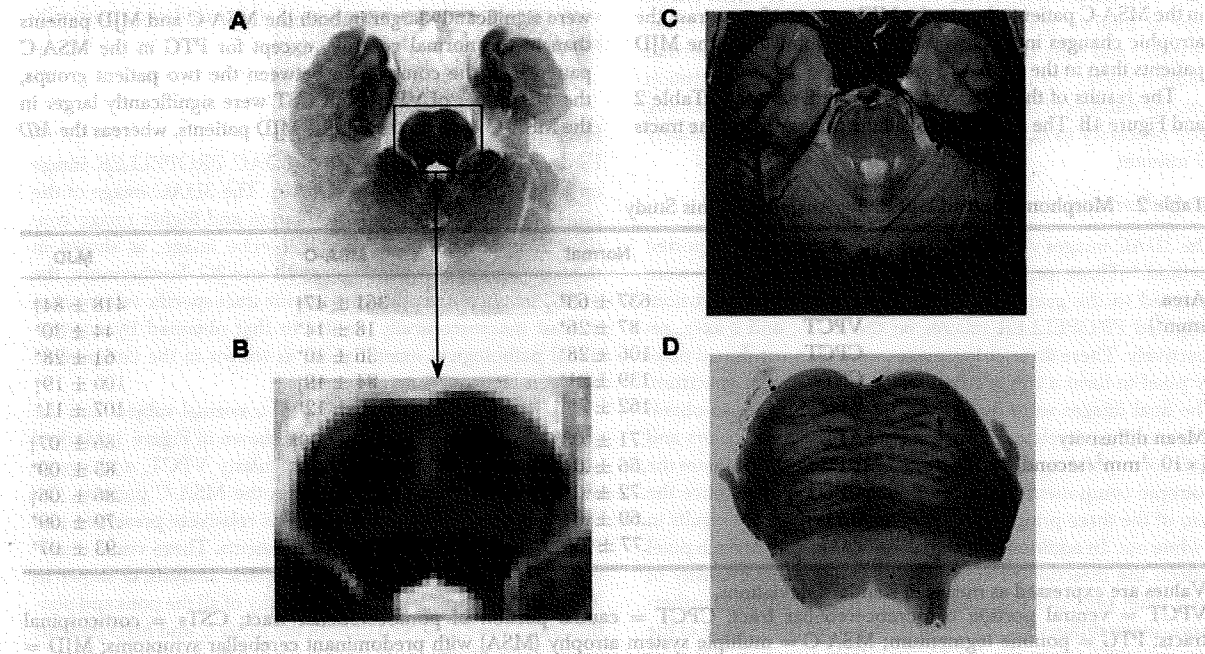

Fig 2. High anatomical resolution and image contrast of 3DAC PROPELLER image on 3.0T system. A: 3DAC PROPELLER image of healthy volunteer on 3.0T system, B: magnified 3DAC image of pons, indicated by a rectangle in A, C: conventional fast spin-echo T2-wieghted image of healthy volunteer on 3.0T system, D: Kluver-Barrera staining of normal pons.

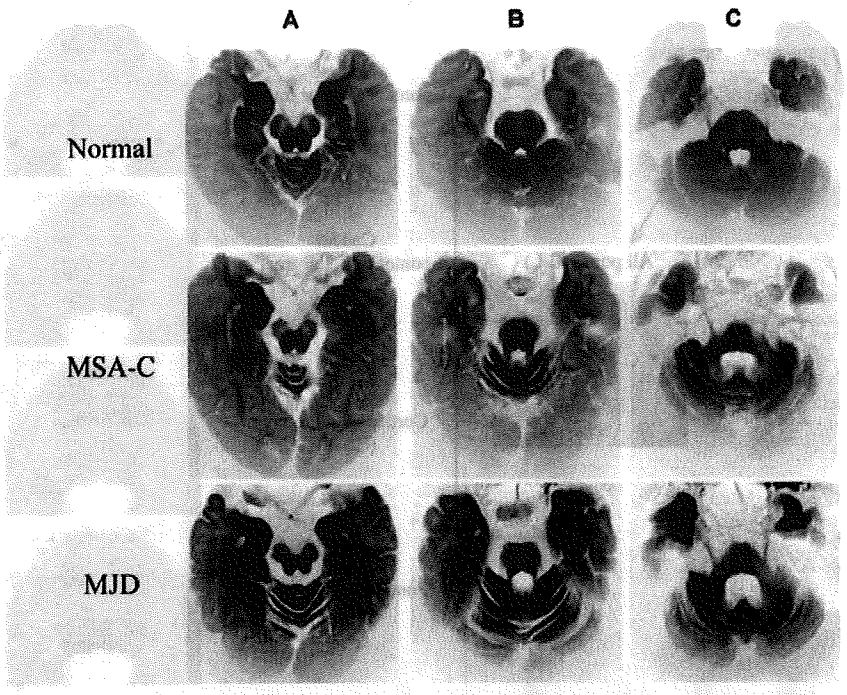

Fig 3. Representative 3DAC PROPELLER images of lower midbrain (A), upper pons (B) and middle pons (C) on 3.0T system of normal controls, patients with multiple system atrophy with predominant cerebellar symptoms (MSA-C) and patients with Machado-Joseph disease (MJD). On the slice of the middle pons, marked atrophy of the ventral portion of the pontocerebellar tract (VPCT) and severe atrophy of the middle cerebellar peduncles are observed in the MSA-C patients. In contrast, VPCT is relatively preserved in the MJD patients, although the area of the pons is reduced as much as that in the case of the MSA-C patients.

in the MSA-C patients than in the MJD patients. In contrast, the atrophic changes in PTG were more pronounced in the MJD patients than in the MSA-C patients.

The results of the diffusivity analysis are shown in Table 2 and Figure 4B. The *MD* values of all the pons and pontine tracts were significantly larger in both the MSA-C and MJD patients than in the normal controls, except for PTG in the MSA-C patients. In the comparison between the two patient groups, the *MD* values of VPCT and CST were significantly larger in the MSA-C patients than in the MJD patients, whereas the *MD*

Table 2. Morphometric and Diffusivity Analyses in This Study

		Normal	MSA-C	MJD
Area (mm^2)	ALL	637 ± 63*	361 ± 47†	418 ± 84†
	VPCT	87 ± 26*	18 ± 14*	44 ± 30*
	CPCT	106 ± 28*	36 ± 10*	61 ± 28*
	CSTs	139 ± 21*	84 ± 19†	100 ± 19†
	PTG	162 ± 7*	126 ± 12*	107 ± 11*
Mean diffusivity ($\times 10^{-3} mm^2$/second)	ALL	.71 ± .03*	.90 ± .06†	.86 ± .07†
	VPCT	.66 ± .04*	1.04 ± .20*	.83 ± .09*
	CPCT	.72 ± .04*	.91 ± .06†	.86 ± .06†
	CSTs	.69 ± .04*	.86 ± .07*	.79 ± .09*
	PTG	.77 ± .04‡	.82 ± .09‡	.93 ± .07*

Values are expressed as means ± standard deviations.
VPCT = ventral portion of pontocerebellar tract; CPCT = caudal portion of pontocerebellar tract; CSTs = corticospinal tracts; PTG = pontine tegmentum; MSA-C = multiple system atrophy (MSA) with predominant cerebellar symptoms; MJD = Machado-Joseph disease.
*Significantly different ($P < .05$) from the other two groups.
†Significantly different ($P < .05$) from normal controls.
‡Significantly different ($P < .05$) from MJD patients.

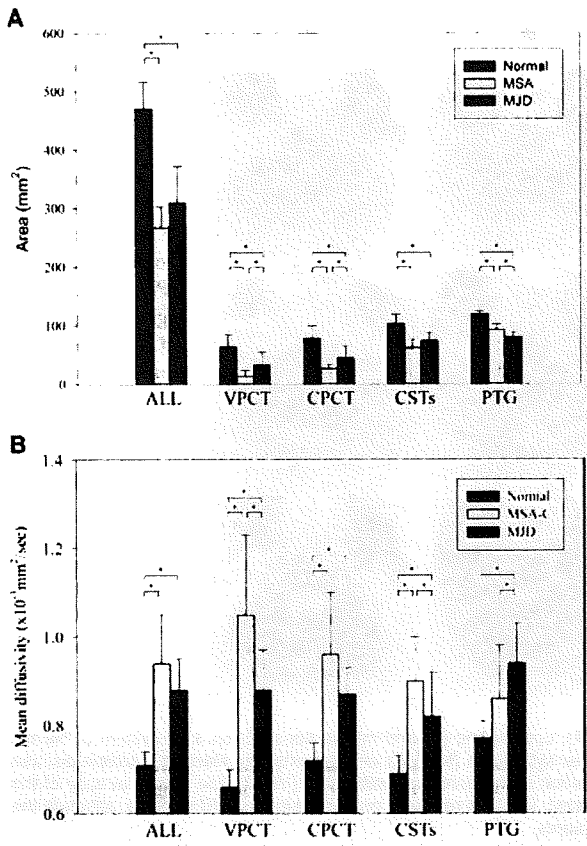

Fig 4. Bar charts with error bars of area values (A) and mean diffusivity values (B) of all pons (ALL), ventral portion of pontocerebellar tract (VPCT), caudal portion of pontocerebellar tract (CPCT), corticospinal tracts (CSTs), and pontine tegmentum (PTG) in normal controls, patients with multiple system atrophy with predominant cerebellar symptoms (MSA-C) and patients with Machado-Joseph disease (MJD). Each bar indicates mean, and each error bar indicates standard deviation. *Significantly different ($P < .05$).

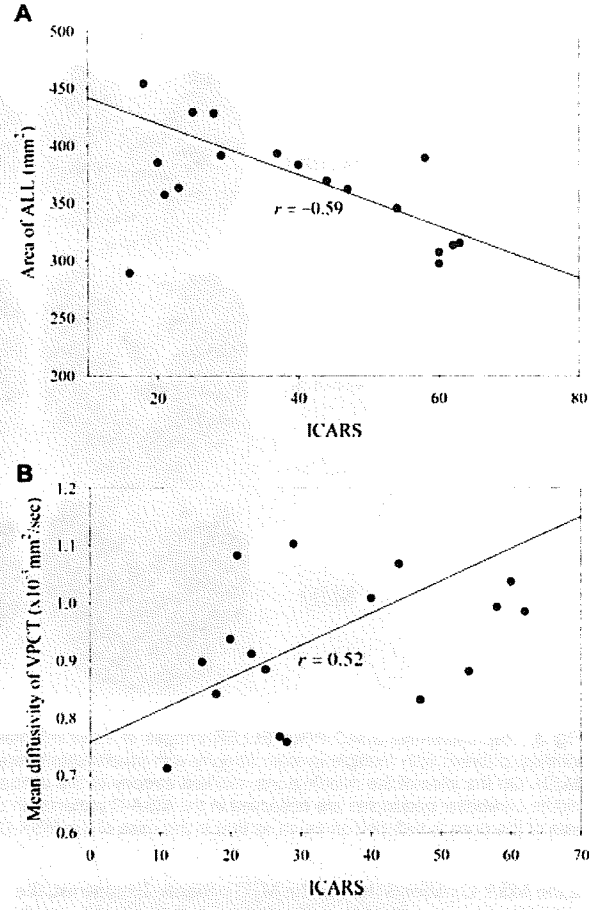

Fig 5. Scatter plots of International Cooperative Ataxia Rating Scale (ICARS) scores versus area measurements of all pons (ALL) (A), and mean diffusivity values of ventral portion of pontocerebellar tract (VPCT) (B) of all patients, with linear regression lines given by Pearson's correlation test ($P < .05$). The correlation coefficients (r) of the test are also indicated.

values of PTG were significantly larger in the MJD patients than in the MSA-C patients.

In all the patients with both MSA-C and MJD, there was a significant negative correlation between the area measurements of all the pons and the ICARS scores ($r = -.59$, Fig 5A). In addition, the *MD* values of VPCT in all the patients also significantly correlated with the ICARS scores of the patients ($r = .52$, Fig 5B).

Discussion

This study has a distinctive new feature, that is, "tract by tract" analysis in vivo of pontine degeneration in SCD. Although there have been previous studies focusing on individual tract degeneration in SCD found in the literature such as the qualitative analysis of transverse pontine fibers using diffusion- and T2-weighted imaging,[15] or diffusion-weighted and diffusion tensor imaging of cerebellar peduncles,[16-19] our study has the advantages of comprehensive and quantitative analyses of the pontine tracts involved in degenerative processes in SCD. The success of this study is largely attributed to the acquisition of a 3DAC PROPELLER image of the pons on a 3.0T system. The process of tract identification carried out in this study definitely cannot be achieved using a conventional gray-scale MR image, as shown in Figure 2. The true color image of the pons with higher anatomical resolution and higher image contrast only allows for precise automatic tract identification with complete reproducibility for reliable morphometric and diffusivity analyses.

Another advantage of this study is that we were able to perform both morphometric and diffusivity analyses for evaluating pontine tract degeneration using a single imaging technique, namely, 3DAC PROPELLER. The method using a combination of two types of analysis enables a more accurate characterization of disease processes than other methods using only one type of analysis.

First, morphometric analysis provides information on the pathological changes of pontine tracts in a macroscopic viewpoint, namely, the atrophy of each tract. The current analysis showed that the atrophic changes in VPCT and CPCT were more pronounced in the MSA-C patients than in the MJD patients despite the fact that these two patient groups were matched for the severities of the cerebellar symptoms, whereas the atrophic change in PTG was more pronounced in the MJD patients than in the MSA-C patients; these results are consistent with previous pathological findings,[20-22] the results of previous morphometric studies using conventional imaging techniques,[23-29] and the results of earlier studies by voxel-based morphometry.[30-36]

On the other hand, diffusivity analysis provides information on the pathological changes of pontine tracts in a microscopic viewpoint, namely, the change in water molecule diffusivity. As reported previously,[16-19,37-43] the current analysis also showed significantly increased *MD* values of all the pons in the MSA and MJD patients when compared with the normal controls. This result indicates that the pontine tracts of the patients contained chronically degenerated axons reflected as increased extracellular spaces associated with axonal loss, neuronal loss, and gliosis.[44] More importantly, the diffusivity analysis in this study showed that the increase in *MD* differed in degree depending on each pontine tract in each disease. In the comparison between the two patient groups, the *MD* values of VPCT and CST were significantly larger in the MSA-C patients than in the MJD patients, whereas the *MD* values of PTG were significantly larger in the MJD patients than in the MSA-C patients. Instead of the 3DAC PROPELLER used in this study, diffusion tensor imaging (DTI) using a PROPELLER sequence may provide more detailed information on the diffusion characteristics in the pontine tracts, although the scanning time for the DTI using a PROPELLER sequence increases to approximately 30 minutes. We believe that 3DAC PROPELLER is the best compromise providing both an acceptable scanning time for a routine clinical examination and an excellent image quality provided by PROPELLER imaging.

Furthermore, note that the results of the diffusivity analysis were in good agreement with those of the morphometric analysis. The combination of the two types of analysis showed that tract-specific changes in atrophy and diffusivity were observed in the pons, and that the specific characteristics of the changes clearly delineated the pathologies of MSA-C and MJD. Atrophy and increased diffusivity of the dorsal portion of the pons indicated MSA-C, whereas atrophy and increased diffusivity of PTG indicated MJD.

The correlation analyses of the ICARS scores of all the patients with the area measurements or *MD* values in each tract showed that the severities of the cerebellar symptoms of the patients correlated well with both the severities of the pontine atrophy and the *MD* values of the ventral pontocerebellar tracts. These results were consistent with those of a previous study using DTI showing that the fractional anisotropy values of MCPs inversely correlate with the ICARS scores of MSA patients.[16] Because the pontocerebellar tracts create afferent pathways running through the middle cerebellar peduncles to the cerebellar cortex, it is reasonable to assume that degenerative changes in pontocerebellar tracts correlate well with the severity of cerebellar symptoms. Therefore, the parameters obtained from this study, namely, the area measurement and *MD* value are useful for monitoring the disease severity of patients with SCD.

We should address a couple of technical problems in our method here. One is the higher specific absorption rate caused by using a PROPELLER sequence, which is particularly remarkable at 3.0T. As a result, the number of slices used in this study is limited to four. The other problem is the relatively long scanning time for obtaining PROPELLER diffusion-weighted images. Recently, a diffusion-weighted echo planar imaging (EPI) sequence has been combined with a newly developed parallel imaging technique[45] to reduce the amount of susceptibility artifacts. These problems may be solved in the future if this modified EPI technique can produce a diffusion-weighted image of the brainstem with higher image quality that is comparable to, if not superior to, that of the PROPELLER technique.

In conclusion, this study demonstrated that 3DAC PROPELLER on a 3.0T system, which has definite advantages over previous imaging techniques, enables in vivo "tract by tract" quantitative analysis of pontine degeneration in SCD. We hope that this powerful imaging technique, once it becomes available in ordinary clinical settings, will be of great help for discriminating and monitoring degenerative disease processes in SCD.

This study was supported by grants from the Ministry of Education, Culture, Sports, Science and Technology (Japan) and a grant for the promotion of the University of Niigata Research Projects (Japan).
The authors thank Drs. S. Hayashi, A. Kakita, and H. Takahashi (Department of Pathology, Brain Research Institute, University of Niigata, Niigata, Japan) for preparing the pathological specimens used in this study.

References

1. Nakada T, Matsuzawa H, Kwee IL. Magnetic resonance axonography of the rat spinal cord. *Neuroreport* 1994;5:2053-2056.
2. Nakada T, Matsuzawa H. Three-dimensional anisotropy contrast magnetic resonance imaging of the rat nervous system: MR axonography. *Neurosci Res* 1995;22:389-398.
3. Matsuzawa H, Kwee IL, Nakada T. Magnetic resonance axonography of the rat spinal cord: postmortem effects. *J Neurosurg* 1995;83:1023-1028.
4. Igarashi H, Katayama Y, Tsuganezawa T, Yamamuro M, Terashi A, Owan C. Three-dimensional anisotropy contrast (3DAC) magnetic resonance imaging of the human brain: application to assess Wallerian degeneration. *Intern Med* 1998;37:662-668.
5. Nakada T, Nakayama N, Fujii Y, Kwee IL. Clinical application of three-dimensional anisotropy contrast magnetic resonance axonography. Technical note. *J Neurosurg* 1999;90:791-795.
6. Watanabe T, Honda Y, Fujii Y, Koyama M, Matsuzawa H, Tanaka R. Three-dimensional anisotropy contrast magnetic resonance axonography to predict the prognosis for motor function in patients suffering from stroke. *J Neurosurg* 2001;94:955-960.
7. Kamada K, Houkin K, Iwasaki Y, et al. Rapid identification of the primary motor area by using magnetic resonance axonography. *J Neurosurg* 2002;97:558-567.
8. Watanabe T, Honda Y, Fujii Y, Koyama M, Tanaka R. Serial evaluation of axonal function in patients with brain death by

using anisotropic diffusion-weighted magnetic resonance imaging. *J Neurosurg* 2004;100:56-60.
9. Nakada T, Matsuzawa H, Fujii Y, Takahashi H, Nishizawa M, Kwee IL. Three-dimensional anisotropy contrast periodically rotated overlapping parallel lines with enhanced reconstruction (3DAC PROPELLER) on a 3.0T system: a new modality for routine clinical neuroimaging. *J Neuroimaging* 2006;16:206-211.
10. Gilman S, Low PA, Quinn N, et al. Consensus statement on the diagnosis of multiple system atrophy. *J Neurol Sci* 1999;163:94-98.
11. Trouillas P, Takayanagi T, Hallett M, et al. International Cooperative Ataxia Rating Scale for pharmacological assessment of the cerebellar syndrome. The Ataxia Neuropharmacology Committee of the World Federation of Neurology. *J Neurol Sci* 1997;145:205-211.
12. Pipe JG. Motion correction with PROPELLER MRI: application to head motion and free-breathing cardiac imaging. *Magn Reson Med* 1999;42:963-969.
13. Pipe JG, Farthing VG, Forbes KP. Multishot diffusion-weighted FSE using PROPELLER MRI. *Magn Reson Med* 2002;47:42-52.
14. Basser PJ. Inferring microstructural features and the physiological state of tissues from diffusion-weighted images. *NMR Biomed* 1995;8:333-344.
15. Adachi M, Hosoya T, Yamaguchi K, Kawanami T, Kato T. Diffusion- and T2-weighted MRI of the transverse pontine fibres in spinocerebellar degeneration. *Neuroradiology* 2000;42:803-809.
16. Shiga K, Yamada K, Yoshikawa K, Mizuno T, Nishimura T, Nakagawa M. Local tissue anisotropy decreases in cerebellopetal fibers and pyramidal tract in multiple system atrophy. *J Neurol* 2005;252:589-596.
17. Blain CR, Barker GJ, Jarosz JM, et al. Measuring brain stem and cerebellar damage in parkinsonian syndromes using diffusion tensor MRI. *Neurology* 2006;67:2199-2205.
18. Nicoletti G, Lodi R, Condino F, et al. Apparent diffusion coefficient measurements of the middle cerebellar peduncle differentiate the Parkinson variant of MSA from Parkinson's disease and progressive supranuclear palsy. *Brain* 2006;129:2679-2687.
19. Taoka T, Kin T, Nakagawa H, et al. Diffusivity and diffusion anisotropy of cerebellar peduncles in cases of spinocerebellar degenerative disease. *Neuroimage* 2007;37:387-393.
20. Yuasa T, Ohama E, Harayama H, et al. Joseph's disease: clinical and pathological studies in a Japanese family. *Ann Neurol* 1986;19:152-157.
21. Dürr A, Stevanin G, Cancel G, et al. Spinocerebellar ataxia 3 and Machado-Joseph disease: clinical, molecular, and neuropathological features. *Ann Neurol* 1996;39:490-499.
22. Wenning GK, Tison F, Ben Shlomo Y, Daniel SE, Quinn NP. Multiple system atrophy: a review of 203 pathologically proven cases. *Mov Disord* 1997;12:133-147.
23. Nabatame H, Fukuyama H, Akiguchi I, Kameyama M, Nishimura K, Nakano Y. Spinocerebellar degeneration: qualitative and quantitative MR analysis of atrophy. *J Comput Assist Tomogr* 1988;12:298-303.
24. Schulz JB, Skalej M, Wedekind D, et al. Magnetic resonance imaging-based volumetry differentiates idiopathic Parkinson's syndrome from multiple system atrophy and progressive supranuclear palsy. *Ann Neurol* 1997;110:65-74.
25. Abe Y, Tanaka F, Matsumoto M, et al. CAG repeat number correlates with the rate of brainstem and cerebellar atrophy in Machado-Joseph disease. *Neurology* 1998;51:882-884.
26. Onodera O, Idezuka J, Igarashi S, et al. Progressive atrophy of cerebellum and brainstem as a function of age and the size of the expanded CAG repeats in the MJD1 gene in Machado-Joseph disease. *Ann Neurol* 1998;43:288-296.
27. Murata Y, Yamaguchi S, Kawakami H, et al. Characteristic magnetic resonance imaging findings in Machado-Joseph disease. *Arch Neurol* 1998;64:33-37.
28. Tokumaru AM, Kamakura K, Maki T, et al. Magnetic resonance imaging findings of Machado-Joseph disease: histopathologic correlation. *J Comput Assist Tomogr* 1998;43:241-248.
29. Yoshizawa T, Watanabe M, Frusho K, Shoji S. Magnetic resonance imaging demonstrates differential atrophy of pontine base and tegmentum in Machado-Joseph disease. *J Neurol Sci* 2003;27:45-50.
30. Specht K, Minnerop M, Abele M, Reul J, Wullner U, Klockgether T. In vivo voxel-based morphometry in multiple system atrophy of the cerebellar type. *Arch Neurol* 2003;18:1431-1435.
31. Brenneis C, Seppi K, Schocke MF, et al. Voxel-based morphometry detects cortical atrophy in the Parkinson variant of multiple system atrophy. *Mov Disord* 2003;18:1132-1138.
32. Specht K, Minnerop M, Muller-Hubenthal J, Klockgether T. Voxel-based analysis of multiple-system atrophy of cerebellar type: complementary results by combining voxel-based morphometry and voxel-based relaxometry. *Neuroimage* 2005;25:287-293.
33. Brenneis C, Boesch SM, Egger KE, et al. Cortical atrophy in the cerebellar variant of multiple system atrophy: a voxel-based morphometry study. *Mov Disord* 2006;21:159-165.
34. Hauser TK, Luft A, Skalej M, et al. Visualization and quantification of disease progression in multiple system atrophy. *Mov Disord* 2006;21:1674-1681.
35. Boesch SM, Wolf C, Seppi K, Felber S, Wenning GK, Schocke M. Differentiation of SCA2 from MSA-C using proton magnetic resonance spectroscopic imaging. *J Magn Reson Imaging* 2007;25:564-569.
36. Minnerop M, Specht K, Ruhlmann J, et al. Voxel-based morphometry and voxel-based relaxometry in multiple system atrophy-a comparison between clinical subtypes and correlations with clinical parameters. *Neuroimage* 2007;36:1086-1095.
37. Schocke MF, Seppi K, Esterhammer R, et al. Diffusion-weighted MRI differentiates the Parkinson variant of multiple system atrophy from PD. *Neurology* 2002;58:575-580.
38. Seppi K, Schocke MF, Esterhammer R, et al. Diffusion-weighted imaging discriminates progressive supranuclear palsy from PD, but not from the parkinson variant of multiple system atrophy. *Neurology* 2003;60:922-927.
39. Schocke MF, Seppi K, Esterhammer R, et al. Trace of diffusion tensor differentiates the Parkinson variant of multiple system atrophy and Parkinson's disease. *Neuroimage* 2004;21:1443-1451.
40. Seppi K, Schocke MF, Donnemiller E, et al. Comparison of diffusion-weighted imaging and [123I]IBZM-SPECT for the differentiation of patients with the Parkinson variant of multiple system atrophy from those with Parkinson's disease. *Mov Disord* 2004;19:1438-1445.
41. Kanazawa M, Shimohata T, Terajima K, et al. Quantitative evaluation of brainstem involvement in multiple system atrophy by diffusion-weighted MR imaging. *J Neurol* 2004;251:1121-1124.
42. Ito M, Watanabe H, Kawai Y, et al. Usefulness of combined fractional anisotropy and apparent diffusion coefficient values for detection of involvement in multiple system atrophy. *J Neurol Neurosurg Psychiatry* 2007;78:722-728.
43. Paviour DC, Thornton JS, Lees AJ, Jager HR. Diffusion-weighted magnetic resonance imaging differentiates Parkinsonian variant of multiple-system atrophy from progressive supranuclear palsy. *Mov Disord* 2007;22:68-74.
44. Ueki S, Fujii Y, Matsuzawa H, et al. Assessment of axonal degeneration along the human visual pathway using diffusion trace analysis. *Am J Ophthalmol* 2006;142:591-596.
45. Pruessmann KP, Weiger M, Scheidegger MB, Boesiger P. SENSE: sensitivity encoding for fast MRI. *Magn Reson Med* 1999;42:952-962.

Total deletion and a missense mutation of *ITPR1* in Japanese SCA15 families

K. Hara, MD, PhD
A. Shiga, MMed
H. Nozaki, MD
J. Mitsui, MD
Y. Takahashi, MD, PhD
H. Ishiguro, MD, PhD
H. Yomono, MD, PhD
H. Kurisaki, MD, PhD
J. Goto, MD, PhD
T. Ikeuchi, MD, PhD
S. Tsuji, MD, PhD
M. Nishizawa, MD, PhD
O. Onodera, MD, PhD

Address correspondence and reprint requests to Dr. Osamu Onodera, Department of Molecular Neuroscience, Center for Bioresource-based Researches, Brain Research Institute, Niigata University, 1-757, Asahi-machi-dori, Niigata City 951-8585, Japan
onodera@bri.niigata-u.ac.jp

Supplemental data at www.neurology.org

Editorial, page 542

ABSTRACT

Background: Spinocerebellar ataxia type 15 (SCA15) is a progressive neurodegenerative disorder characterized by pure cerebellar ataxia, very slow progression, and distinct cerebellar atrophy. The locus for SCA15 was first mapped to 3p24.2-3pter in an Australian family. We have subsequently mapped two Japanese families presenting with ataxia and postural tremor of the head, arm, or trunk to the SCA15 locus. Recently, partial deletions involving both the type 1 inositol 1,4,5-triphosphate receptor (*ITPR1*) and sulfatase modifying factor 1 (*SUMF1*) genes have been identified in Australian and British families with SCA15.

Methods: We conducted fine haplotype analysis on the region including *ITPR1*. To identify the deletion, we conducted gene dosage analysis and array-based comparative genomic hybridization (aCGH) analysis. Gene expression analysis was performed using quantitative real-time reverse transcription PCR. Mutational analyses of *ITPR1* and *SUMF1* were also performed.

Results: We have identified a 414-kb deletion including the entire *ITPR1* and exon 1 of *SUMF1* in patients in family A. The expression levels of *ITPR1* and *SUMF1* mRNAs of the patient were half those of the normal control. Furthermore, in family B, we have identified a C-to-T substitution at position 8581 of *ITPR1*, resulting in the amino acid substitution of leucine for proline at codon 1059, which is highly conserved among species.

Conclusions: Our results strongly confirm that *ITPR1* is the causative gene for SCA15 and suggest that we need to investigate the point mutation in *ITPR1* in the patients with autosomal dominant cerebellar ataxia and tremor. ***Neurology*® 2008;71:547-551**

GLOSSARY

aCGH = array-based comparative genomic hybridization; **LCR** = low-copy repeat; **NAHR** = nonallelic homologous recombination; **NHEJ** = nonhomologous end joining; **SCA15** = spinocerebellar ataxia type 15.

Spinocerebellar ataxia type 15 (SCA15) was first reported on the basis of a single large Australian family with pure cerebellar ataxia, very slow progression, and marked cerebellar atrophy, particularly in the vermis.[1,2] The disease locus was mapped to chromosome 3p24.2-3pter.[1,2] We have subsequently identified two Japanese families with autosomal dominant cerebellar ataxia characterized by postural and action tremor. The disease locus for these Japanese SCA families was mapped to 3p25.3-26.1 with the highest cumulative multipoint lod score of 3.30 at D3S3728.[3] Interestingly, the critical region for our families partly overlapped with the locus for the Australian SCA15 family. The overlapping region was 7.9 cM between D3S1620 and D3S1304. Clinical features, including a very slow progression, tremor of the head, arm, or trunk and distinct cerebellar atrophy without brainstem atrophy, are shared among these fam-

e-Pub ahead of print on June 25, 2008, at www.neurology.org.

From the Department of Neurology (K.H., A.S., H.N., M.N.), Brain Research Institute, and Department of Molecular Neuroscience (A.S., H.N., T.I., O.O.), Center for Bioresource-based Researches, Brain Research Institute, Niigata University, Niigata City; Department of Neurology (J.M., Y.T., J.G., S.T.), Division of Neuroscience, Graduate School Medicine, University of Tokyo; Department of Neurology (H.I.), Akita Red Cross Hospital, Akita City; and Department of Neurology (H.Y., H.K.), National Tokyo Hospital, Japan.

Supported in part by KAKENHI (Grant-in-Aid for Scientific Research) on Priority Areas "Advanced Brain Science Project," "Applied Genomics," the 21st Century COE Program "Center for Integrated Brain Medical Science," and a Grant-in-Aid for Scientific Research (A) and (B) from the Ministry of Education, Culture, Sports, Science and Technology of Japan, a grant for the Research for the Future Program from the Japan Society for the Promotion of Science, a grant for "the Research Committee for Ataxic Diseases" of the Research on Measures for Intractable Diseases from the Ministry of Health, Labor and Welfare, Japan, Grant for Promotion of Niigata University Research Projects, and Grant-in-Aid for Young Scientists (B).

Disclosure: The authors report no disclosures.

ilies, raising the possibility that the causative gene for the Australian SCA15 family is allelic to that for the two Japanese SCA15 families.[1] However, some of the clinical features of the Japanese families are distinct from those of the Australian family as regards to the extracerebellar signs. Postural tremor of the head, arm, or trunk is more predominant in the Japanese patients than in the Australian patients.[3] Subsequently, additional families have been reported to link to the SCA15 locus.[4]

Recently, partial deletions of type 1 inositol 1,4,5-triphosphate receptor (*ITPR1*) and sulfatase modifying factor 1 (*SUMF1*) genes have been identified in the Australian SCA15 family and two British families with pure cerebellar ataxia, suggesting that *ITPR1* is the causative gene for SCA15.[5] Furthermore, a partial deletion of *ITPR1* has been identified in the Japanese SCA16 family.[6] However, it is unclear whether *ITPR1* is solely responsible for SCA15, because the deletions also involve *SUMF1*. Here, we report that the two families mapped to the SCA15 locus have the mutations in *ITPR1*, including a missense mutation, which strongly confirms that *ITPR1* is the causative gene for SCA15.

METHODS SCA families. The family members of the two Japanese families mapped to the SCA15 locus were analyzed in the present study. In addition, 54 autosomal dominant SCA families in which abnormal expansions of CAG repeats in the responsible genes for SCA1, SCA2, Machado-Joseph disease/SCA3, SCA6, SCA8, SCA17, and dentatorubral-pallidoluysian atrophy have been excluded are also enrolled for gene copy number analysis of *ITPR1*. High-molecular-weight genomic DNA was extracted from peripheral leukocytes after obtaining informed consent from the patients. The present study was approved by the Institutional Review Board of Niigata University.

Genetic analysis. For fine haplotype mapping, we established nine new microsatellite markers, namely, M4439, M4497, M4583, M4667, M4714, M4832, M4919, M4964, and M5757 in the region between D3S3706 and D3S1515 including *ITPR1*. Gene dosage was analyzed using a quantitative real-time PCR technique with the ABI PRISM 7700 Sequence Detection System (Applied Biosystems, Foster City, CA). We also employed the custom high-definition array-based comparative genomic hybridization (aCGH) microarrays (Agilent Technologies Inc., Palo Alto, CA).[7] A region of approximately 3.8 Mb from *CNTN4* (Gene ID: 152330) to D3S1303 was included in the microarray at an average interval of 200 bp for the probes. For gene expression analysis, RNA was extracted from cultured skin fibroblasts from an affected individual (II-4) and a control. The amplified products of all 58 exons of *ITPR1* were subjected to a cycle sequence reaction using BigDye Terminator version 3.0 (Applied Biosystems).[2] Detailed methods are available in table e-1 and e-Methods on the *Neurology*® Web site at www.neurology.org.

RESULTS Identification of deletion involving entire *ITPR1* in family A (Ped 256). To investigate whether a common haplotype is shared among the affected individuals in the two Japanese ataxia families linked to the SCA15 locus,[3] we conducted fine haplotype analyses based on the linkage analysis. We did not find any common founder haplotypes between these Japanese ataxia families. However, all of the affected individuals in family A (Ped 256) lost heterozygosity from M4497 to M4832 (figure 1A). Furthermore, alleles from M4583 to M4832 were not transmitted from the affected individual II-5 to his affected daughter III-3 (figure 1A). These findings strongly suggested that the affected individuals in this family (Ped 256) had a heterozygous deletion in the region containing two genes: *ITPR1* and *SUMF1* (figure e-1A). We performed quantitative real-time PCR analyses for *ITPR1* and *SUMF1*. The dosages of exons 2, 26, and 58 of *ITPR1* and exon 1 of *SUMF1* in the affected individuals were one-half those of unaffected individuals (figure e-1B). These findings indicated that the affected individuals had the deletion of the entire *ITPR1* and exon 1 of *SUMF1*.

Identification of breakpoint sequence in *ITPR1*. To confirm the deletion of *ITPR1*, we performed aCGH analysis using oligonucleotide probes spanning the region from *CNTN4* to D3S1303 on chromosome 3p from three affected individuals (II-5, II-6, and II-8) and two unaffected individuals (II-7 and III-2) in family A. The $\log_2$ R ratios for the affected individuals for the probes from the nucleotide position 4,476,024 to 4,887,327 were decreased to ~ -1, whereas those for the probes from the nucleotide position 4,142,899 to 4,471,831 and from the nucleotide position 4,887,691 to 5,242,899 were ~ 0, confirming the extent of the deletion (figure 1B). In contrast, we detected no deletion in this region in an affected individual in family B (Ped 2216). Furthermore, aCGH analysis was applied to 54 autosomal dominant SCA families; however, no deletion of *ITPR1* or *SUMF1* was detected in these families.

To determine the breakpoint, we developed the primers for each end and performed PCR, obtaining a ~2,300 bp fragment from the affected individuals, but not from the unaffected individuals (figure e-2A). The sequence analysis of this junction fragment revealed that no significant homology was observed when the junction sequence was aligned with the reference genomic sequence at the proximal and distal breakpoints and the sequences at proximal and distal breakpoints showed a two nucleotide overlap (figures e-2B and e-2C). RepeatMasker (http://www.repeatmasker.org/) revealed that

Figure 1 **Deletion analysis of *ITPR1***

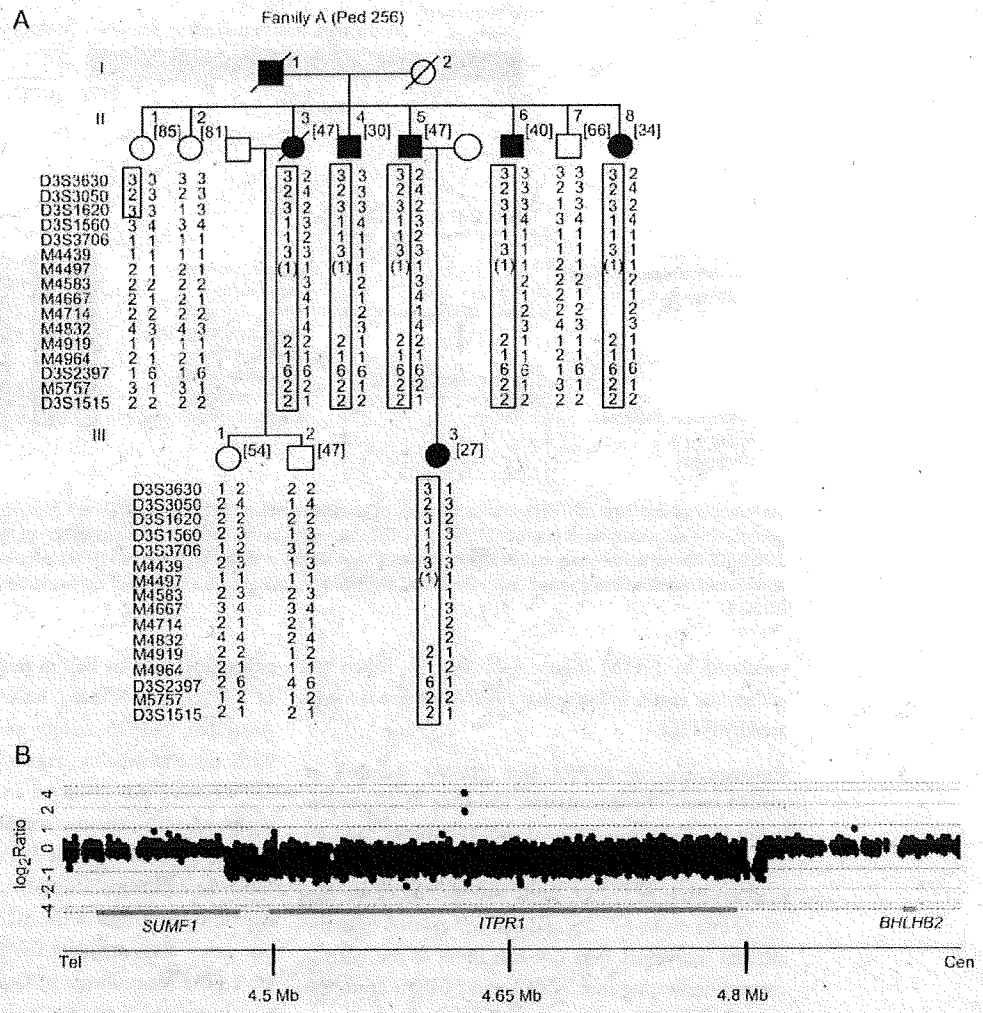

(A) Haplotype analysis of family A (Ped 256) employing microsatellite markers spanning the SCA15 locus at 3p26.1. Squares indicate males. Circles indicate females. Affected individuals are indicated by solid symbols, and unaffected individuals by open symbols. Deceased individuals are indicated by diagonal lines. Age at death or current age are indicated (n in brackets) in unaffected individuals. Age at onset is indicated (n in brackets) in affected individuals. Haplotypes linked to the disease are boxed. It cannot be determined whether the M4497 locus is included in the deletion, since all the affected individuals had the identical allele "1" at M4497; parentheses. (B) Deletion of entire *ITPR1* identified by high-density oligonucleotide array-based CGH analysis. A part of the results of array-based CGH analysis of the affected individual II-5 are plotted as a function of chromosomal position (Mb). Regions of loss (green) and gain (red) are color-coded.

the distal breakpoint was embedded within an AT dinucleotide repeat. The proximal breakpoint was embedded immediately before the *AluSx* element. The deletion in this family is thus 414,018 bp in size, including the entire *ITPR1* and exon 1 of *SUMF1*.

Chromosomal deletion is mainly mediated by two mechanisms: nonallelic homologous recombination (NAHR) or nonhomologous end joining (NHEJ).[8] In the case of NAHR, the chromosomal reengagement occurs between large, highly homologous low-copy repeat (LCR) structures, AT-rich palindromes, and pericentromeric repeats.[8] To determine whether the breakpoints are embedded within LCR structures, we compared the 1-Mb genomic sequence surrounding *SUMF1* and *ITPR1* against itself using PipMaker.[9] The sequence analyses of the junction in our case and those in previously reported cases showed that distal breakpoints were scattered within a ~65 kb region and proximal breakpoints were scattered within a ~223 kbp region[5,6](figure e-3). These breakpoints are frequently embedded within or beside repetitive sequences; however, none of the breakpoints were embedded within LCR structures, AT-rich palindromes, and pericentromeric repeats (figure e-3).[5,6] In addition, the sequences at breakpoints showed a 2–5-nucleotide overlap, which is frequently observed in chromosomal rearrangements

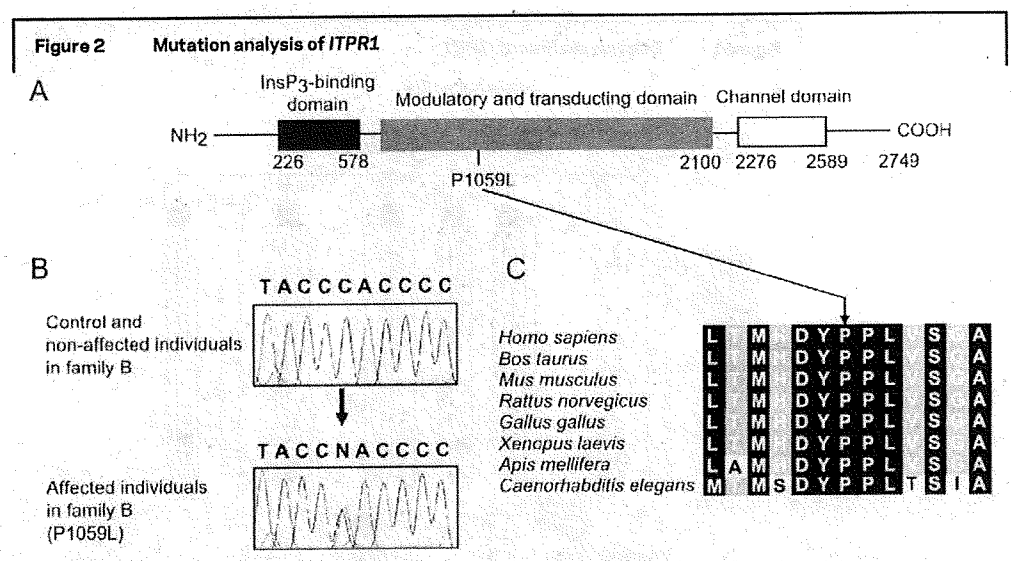

(A) Functional domains of *ITPR1* and location of missense mutation (P1509L). (B) Direct sequencing revealed a heterozygous C-to-T substitution at position 8581 of *ITPR1*, resulting in the amino acid substitution of leucine for proline at codon 1059. (C) Amino acid sequences at the mutation site in *ITPR1* and the orthologs of *ITPR1* aligned by ClustalW. Conserved amino acid residues are shaded using GeneDoc. Each shade represents a degree of conservation (black, 100%; dark gray, 80%).

mediated by NHEJ (figure e-2C).[5,6,10,11] Taken together, the results indicate that *ITPR1* deletion is mediated by NHEJ.

Consequences of *ITPR1* and *SUMF1* deletion at mRNA level. The quantitative real-time PCR analysis using mRNA from cultured skin fibroblasts from an affected individual (II-4) revealed that the mRNA expression levels of *ITPR1* exons 5–6, *ITPR1* exons 25–26, *ITPR1* exons 44–45, and *SUMF1* exons 6–7 of the affected individual were one-half those of the normal control, indicating that *ITPR1* and *SUMF1* from the deleted allele were not expressed (figure e-4).

Identification of missense mutation in *ITPR1* in family B (Ped 2216). We performed nucleotide sequence analyses of the entire exons and splice junctions in *ITPR1* and *SUMF1* of the affected individuals in family B and identified one missense mutation, C8581→T (resulting in substitution of leucine for proline: P1059L) in exon 25 of *ITPR1* in all the affected individuals in the heterozygous state, whereas unaffected individuals did not have this substitution (figure 2, A and B). This nucleotide change was not observed in 234 normal chromosomes in Japanese controls. We found no nucleotide substitutions in *SUMF1*. P1059L was located in the modulatory and transducing domain in *ITPR1* (figure 2A). Amino acid sequence alignment of *ITPR1* using ClustalW[12] revealed that the proline residue at codon 1059 is highly conserved among species (figure 2C).

DISCUSSION In this study, we found the total deletion of *ITPR1* and the decrease in *ITPR1* mRNA expression level by half in family A. Partial deletions of *ITPR1* and *SUMF1* have been reported in one Australian SCA15 family and two British families with pure cerebellar ataxia.[5] Deletions involving *ITPR1* were not observed in the other 54 families with undetermined autosomal dominant ataxia, suggesting that deletions of *ITPR1* are not frequent in Japanese autosomal dominant SCA families. All the deletions identified in the SCA15 families, including our cases, also included *SUMF1*. *SUMF1* is a causative gene for multiple sulfatase deficiency, which is an autosomal recessive disorder characterized by mental retardation, seizure, and leukodystrophy.[13] Patients with a heterozygous mutation in *SUMF1* are clinically healthy, suggesting that the partial deficiency of *SUMF1* does not likely cause neurodegenerative disorders. In addition, in family B, we first identified the missense mutation P1059L in *ITPR1*. Although we did not investigate the function of mutant *ITPR1* with P1059L, we consider that this P1059L mutation causes cerebellar ataxia, because this mutation was not present in 234 chromosomes in Japanese controls and showed complete cosegregation with the disease. Moreover, the mutated proline residue at codon 1059 is highly conserved among species. Recently, a partial deletion of *ITPR1* has been identified in a Japanese SCA16 family.[6] Taken together, these results strongly confirm that *ITPR1* is the responsible gene for cerebellar ataxia in humans.

How do the deletions or the missense mutation of *ITPR1* cause cerebellar ataxia in patients with SCA15? ITPR1 is a major inositol 1,4,5-

triphosphate receptor, which mediates Ca^{2+} release from the endoplasmic reticulum in various neurons, including CA1, basal ganglia, and the thalamic neurons, particularly Purkinje neurons.[14,15] Intracellular Ca^{2+} homeostasis is important for maintaining the function of neurons particularly Purkinje neurons.[16] Indeed, mice homozygous for null *ITPR1* develop ataxia and epilepsy without apparent morphologic abnormalities.[17,18] On the other hand, mice heterozygous for null *ITPR1* develop mild motor discoordinaton without apparent morphologic abnormalities in the cerebellum.[19] Thus, the haploinsufficiency of *ITPR1* may result in dysfunctions confined to Purkinje neurons, and the complete loss of *ITPR1* results in dysfunctions in both cortical and Purkinje neurons. The finding indicates that Purkinje neurons are particularly vulnerable to the gene dosage of *ITPR1*. Indeed, none of the individuals with SCA15 with *ITPR1* mutation had epilepsy or abnormal electroencephalograms, and the clinical phenotype was limited to cerebellar ataxia with tremor even in the elderly.[1-3,5] The neuropathologic findings of individuals with *ITPR1* deletion or missense mutations will confirm this speculation.

Dysregulation of intracellular Ca^{2+} homeostasis by haploinsufficiency or missense mutation of *ITPR1* results in dysfunction of Purkinje neurons, and ultimately might result in degeneration of Purkinje neurons in humans. The study of the molecular mechanism underlying Purkinje cell degeneration caused by *ITPR1* will provide new insights into the mechanism of ataxias and eventually the development of new therapeutic approaches for preventing the degeneration of Purkinje neurons.

Electronic database information. NCBI accession numbers: *Homo sapiens* ITPR1, AAB04947.2; *Bos taurus* ITPR1, NP_777266.1; *Mus musculus* ITPR1, NP_034715.2; *Rattus norvegicus* ITPR1, NP_001007236.1; *Gallus gallus* ITPR1, XP_414438.2; *Xenopus laevis* ITPR1, NP_001084015.1; *Apis mellifera* ITPR1, XP_392236.3; *Caenorhabditis elegans* ITPR1, NP_001023174.1.

Received September 21, 2007. Accepted in final form January 31, 2008.

REFERENCES

1. Gardner RJ, Knight MA, Hara K, Tsuji S, Forrest SM, Storey E. Spinocerebellar ataxia type 15. Cerebellum 2005; 4:47–50.
2. Knight MA, Kennerson ML, Anney RJ, et al. Spinocerebellar ataxia type 15 (sca15) maps to 3p24.2-3pter: exclusion of the ITPR1 gene, the human orthologue of an ataxic mouse mutant. Neurobiol Dis 2003;13:147–157.
3. Hara K, Fukushima T, Suzuki T, et al. Japanese SCA families with an unusual phenotype linked to a locus overlapping with SCA15 locus. Neurology 2004;62:648–651.
4. Dudding TE, Friend K, Schofield PW, Lee S, Wilkinson IA, Richards RI. Autosomal dominant congenital non-progressive ataxia overlaps with the SCA15 locus. Neurology 2004;63:2288–2292.
5. van de Leemput J, Chandran J, Knight MA, et al. Deletion at ITPR1 underlies ataxia in mice and spinocerebellar ataxia 15 in humans. PLoS Genet 2007;3:e108.
6. Iwaki A, Kawano Y, Miura S, et al. Heterozygous deletion of ITPR1, but not SUMF1 in spinocerebellar ataxia type 16. J Med Genet 2007;3:e108.
7. Barrett MT, Scheffer A, Ben-Dor A, et al. Comparative genomic hybridization using oligonucleotide microarrays and total genomic DNA. Proc Natl Acad Sci USA 2004; 101:17765–17770.
8. Shaw CJ, Lupski JR. Implications of human genome architecture for rearrangement-based disorders: the genomic basis of disease. Hum Mol Genet 2004;13 Spec No 1:R57–64.
9. Schwartz S, Zhang Z, Frazer KA, et al. PipMaker: a web server for aligning two genomic DNA sequences. Genome Res 2000;10:577–586.
10. Henthorn PS, Smithies O, Mager DL. Molecular analysis of deletions in the human beta-globin gene cluster: deletion junctions and locations of breakpoints. Genomics 1990;6:226–237.
11. Toffolatti L, Cardazzo B, Nobile C, et al. Investigating the mechanism of chromosomal deletion: characterization of 39 deletion breakpoints in introns 47 and 48 of the human dystrophin gene. Genomics 2002;80:523–530.
12. Thompson JD, Higgins DG, Gibson TJ. CLUSTAL W: improving the sensitivity of progressive multiple sequence alignment through sequence weighting, position-specific gap penalties and weight matrix choice. Nucleic Acids Res 1994;22:4673–4680.
13. Cosma MP, Pepe S, Annunziata I, et al. The multiple sulfatase deficiency gene encodes an essential and limiting factor for the activity of sulfatases. Cell 2003;113: 445–456.
14. Nakanishi S, Maeda N, Mikoshiba K. Immunohistochemical localization of an inositol 1,4,5-trisphosphate receptor, P400, in neural tissue: studies in developing and adult mouse brain J Neurosci 1991;11:2075–2086.
15. Sharp AH, Nucifora FC, Jr, Blondel O, et al. Differential cellular expression of isoforms of inositol 1,4,5-triphosphate receptors in neurons and glia in brain. J Comp Neurol 1999;406:207–220.
16. Hartmann J, Konnerth A. Determinants of postsynaptic Ca2+ signaling in Purkinje neurons. Cell Calcium 2005; 37:459–466.
17. Matsumoto M, Nagata E. Type 1 inositol 1,4,5-trisphosphate receptor knock-out mice: their phenotypes and their meaning in neuroscience and clinical practice. J Mol Med 1999;77:406–411.
18. Matsumoto M, Nakagawa T, Inoue T, et al. Ataxia and epileptic seizures in mice lacking type 1 inositol 1,4,5-trisphosphate receptor. Nature 1996;379:168–171.
19. Ogura H, Matsumoto M, Mikoshiba K. Motor discoordination in mutant mice heterozygous for the type 1 inositol 1,4,5-trisphosphate receptor. Behav Brain Res 2001;122: 215–219.

We thank the clinical, genetic, pathology, and technical staff of the collaborating centers for making information and DNA/tissue samples available for this study. We also thank the families of patients whose generosity made this research possible.

References

1. Arai T, Hasegawa M, Akiyama H, et al. TDP-43 is a component of ubiquitin-positive tau-negative inclusions in frontotemporal lobar degeneration and amyotrophic lateral sclerosis. Biochem Biophys Res Commun 2006;351:602–611.
2. Neumann M, Sampathu DM, Kwong LK, et al. Ubiquitinated TDP-43 in frontotemporal lobar degeneration and amyotrophic lateral sclerosis. Science 2006;314:130–133.
3. Cairns NJ, Neumann M, Bigio EH, et al. TDP-43 in familial and sporadic frontotemporal lobar degeneration with ubiquitin inclusions. Am J Pathol 2007;171:227–240.
4. Mackenzie IRA, Bigio EH, Ince PG, et al. Pathological TDP-43 distinguishes sporadic amyotrophic lateral sclerosis from amyotrophic lateral sclerosis with SOD1 mutations. Ann Neurol 2007;61:427–434.
5. Siddique T, Lalani I. Genetic aspects of amyotrophic lateral sclerosis. Adv Neurol 2002;88:21–32.
6. Pasinelli P, Brown RH. Molecular biology of amyotrophic lateral sclerosis: insights from genetics. Nat Rev Neurosci 2006;7:710–723.
7. Goate A, Chartier-Harlin MC, Mullan M, et al. Segregation of a missense mutation in the amyloid precursor protein gene with familial Alzheimer's disease. Nature 1991;349:704–706.
8. Polymeropoulos MH, Lavedan C, Leroy E, et al. Mutation in the alpha-synuclein gene identified in families with Parkinson's disease. Science 1997;276:2045–2047.
9. Hutton M, Lendon CL, Rizzu P, et al. Association of missense and 5′-splice-site mutations in tau with the inherited dementia FTDP-17. Nature 1998;393:702–705.
10. Wang HY, Wang IF, Bose J, Shen CK. Structural diversity and functional implications of the eukaryotic TDP gene family. Genomics 2004;83:130–139.
11. Ou SH, Wu F, Harrich D, et al. Cloning and characterization of a novel cellular protein, TDP-43, that binds to human immunodeficiency virus type 1 TAR DNA sequence motifs. J Virol 1995;69:3584–3596.
12. Buratti E, Dork T, Zuccato E, et al. Nuclear factor TDP-43 and SR proteins promote in vitro and in vivo CFTR exon 9 skipping. EMBO J 2001;20:1774–1784.
13. Ayala YM, Pantano S, D'Ambrogio A, et al. Human, Drosophila, and *C. elegans* TDP43: nucleic acid binding properties and splicing regulatory function. J Mol Biol 2005;348:575–588.
14. Cairns NJ, Bigio EH, Mackenzie IRA, et al. Neuropathologic diagnostic and nosologic criteria for frontotemporal lobar degeneration: consensus of the Consortium for Frontotemporal Lobar Degeneration. Acta Neuropathol 2007;114:5–22.

TDP-43 Mutation in Familial Amyotrophic Lateral Sclerosis

Akio Yokoseki, MD,[1] Atsushi Shiga, Mmed,[1,2] Chun-Feng Tan, MD, PhD,[3] Asako Tagawa, MD,[1] Hiroyuki Kaneko, Mmed,[1,2] Akihide Koyama, Mmed,[1,2] Hiroto Eguchi, MD,[4] Akira Tsujino, MD,[4] Takeshi Ikeuchi, MD, PhD,[2] Akiyoshi Kakita, MD, PhD,[3] Koichi Okamoto, MD, PhD,[5] Masatoyo Nishizawa, MD, PhD,[1] Hitoshi Takahashi, MD, PhD,[3] and Osamu Onodera, MD, PhD[2]

Amyotrophic lateral sclerosis (ALS) is a fatal neurodegenerative disorder. Accumulating evidence has shown that 43kDa TAR-DNA–binding protein (TDP-43) is the disease protein in ALS and frontotemporal lobar degeneration. We previously reported a familial ALS with Bumina bodies and TDP-43-positive skein-like inclusions in the lower motor neurons; these findings are indistinguishable from those of sporadic ALS. In three affected individuals in two generations of one family, we found a single base-pair change from A to G at position 1028 in TDP-43, which resulted in a Gln-to-Arg substitution at position 343. Our findings provide a new insight into the molecular pathogenesis of ALS.

Ann Neurol 2008;63:538–542

Amyotrophic lateral sclerosis (ALS) is a fatal and incurable neurodegenerative disorder. One of the neuropathological hallmarks of ALS is the presence of ubiquitinated neuronal cytoplasmic inclusions (NCIs) in lower motor neurons.[1,2] Recently, the 43kDa TAR-DNA–binding protein (TDP-43) has been identified as the major component of NCIs in sporadic ALS (SALS) and superoxide dismutase 1 (SOD1)–negative familial ALS (FALS), as well as sporadic and familial frontotemporal lobar dementia (FTLD).[3–7] Furthermore, the abnormal-molecular-weight fragments of TDP-43 were

From the Departments of [1]Neurology, [2]Molecular Neuroscience, and [3]Pathology, Brain Research Institute, Niigata University, Niigata; [4]First Department of Internal Medicine, Nagasaki University Graduate School of Biomedical Sciences, Nagasaki; and [5]Department of Neurology, Gunma University Graduate School of Medicine, Maebashi, Japan.

Received Oct 9, 2007, and in revised form Feb 23, 2008. Accepted for publication Feb 27, 2008.

A.Y. and A.S. contributed equally to this article.

Published online in Wiley InterScience (www.interscience.wiley.com). DOI: 10.1002/ana.21392

Address correspondence to Dr Onodera and Dr. Takahashi, Brain Research Institute, Niigata University, Chuo-ku, Asahi-machi-don, Niigata 951-85858, Japan. E-mail onodera@bn.niigata-u.ac.jp, hitoshi@niigata-u.ac.jp

